EPSC2017

TP5/OPS5/SB14 abstracts

EPSC Abstracts
Vol. 11, EPSC2017-326, 2017
European Planetary Science Congress 2017

Deep dyke exposures in northern Valles Marineris highlight the significance of erosion in chasma genesis

D. Mège (1), J. Gurgurewicz (2,1) and O. Bourgeois (3)
(1) Space Research Centre, Polish Academy of Sciences, Warsaw, Poland (dmege@cbk.waw.pl), (2) Institute of Geological Sciences, Polish Academy of Sciences, Research Centre in Wroclaw, Poland (jgur@cbk.waw.pl), (3) Planetology and Geodynamics Laboratory, CNRS UMR 6112, University of Nantes, France (olivier.bourgeois@univ-nantes.fr)

Abstract

The formation of the deep northern Valles Marineris troughs is conjectural [e.g., 1]. We report on a dyke swarm exposed on the floor of Ophir Chasma, one of the northern Valles Marineris troughs. Dyke thickness is commonly tens of meters, similar to dykes exposed in continental shields on Earth, and suggest erosion of kilometers of rocks above them. Glacial erosion is the most likely erosional process.

1. Introduction

An extensive survey of the floor of Ophir Chasma reveals exposures of a deep dyke swarm, the Ophir Chasma Dyke Swarm (ODS), suggesting that magmatic dilation as well as erosion significantly contributed to trough deepening.

2. Ophir Chasma Dyke Swarm

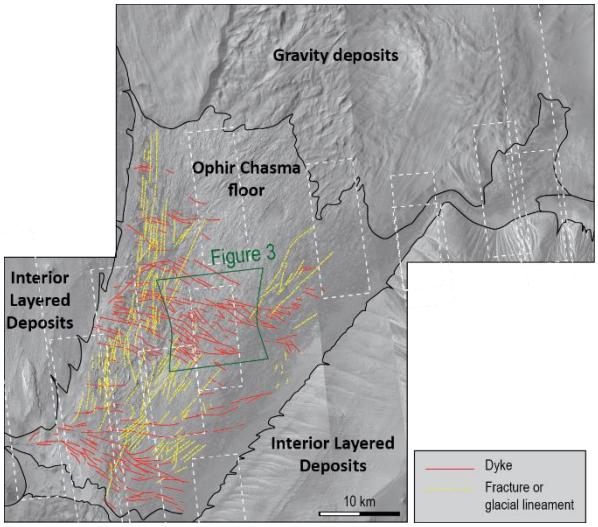

Figure 1: The Ophir Chasma Dyke Swarm (red). The background image is a CTX image mosaic (5 m/pixel). HiRISE footprints are in white.

The Ophir Chasma floor displays a dense network of dykes (Figure 1), which can be observed in the visible spectral range on CTX (5 m/pixel) and HiRISE (25 cm/pixel) images. Many of them are several tens of meters thick. CRISM spectral data analysis reveals a mafic composition, with Mg-rich olivine and high-Ca pyroxene. In some areas, dykes show a sulfate-rich spectral signature taken as testimony of hydrothermal weathering [2], rather than transportation of sulfates weathered from chasma walls.

3. Implications for chasma formation mechanisms

Dyke thickness primarily depends on the Young's modulus of the host rock, which increases with hydrostatic pressure, hence globally, with depth. The widespread occurrence of dykes several tens of meters thick on the floor of Ophir Chasma suggests that the current exposure level is closer to the level of neutral buoyancy of Martian mafic magmas, estimated to ca. 11 km [3], than to the surface. Exposure of dikes emplaced at such depths requires that the exposed chasma floor has been intensely eroded after their emplacement.

4. Erosional systems

Rivers. In most geomorphological systems, where erosion and deposition are controlled by subaerial river networks, large depressions are the locus of thick sedimentary infillings. Depressions that match the dimensions of the Valles Marineris chasmata on Earth include rifts as well as mountain foreland basins, which are fed by river networks and are commonly filled by kilometers of sediments. The observations reported here are not consistent with such systems, which would deeply bury any dyke intruded in the basement.

Glaciers. Subglacial erosion by ice and meltwater is a process that allows to carve valleys efficiently without filling the floor with thick sediments. Pervasive glacial landscapes were demonstrated in Valles Marineris, where past and fossil valley glaciers have been identified [4, 5]. We suggest that the floor of the central Ophir Chasma may have followed an evolution similar to the bedrock of Antarctic ice streams (Figure 2). Its current low elevation would thus result from a combination of dyke dilation and tectonic stretching, and subglacial erosion over kilometers.

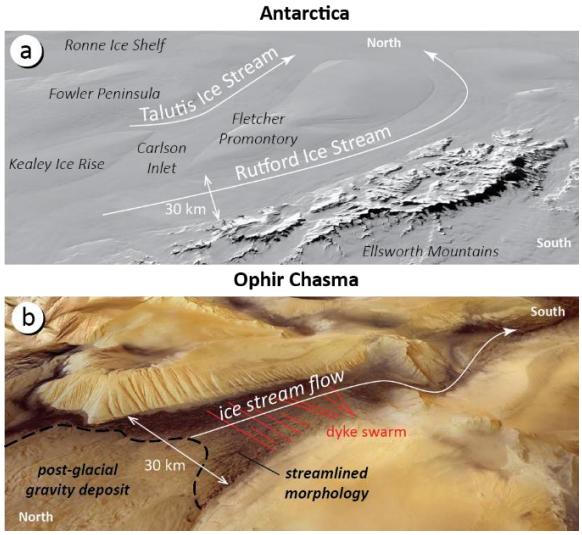

Figure 2: A former ice stream may have filled Ophir Chasma (b) and eroded the bedrock over several kilometers, following processes that are currently active in Antarctica, with (a) the example of the Rutford Ice Stream [6].

Bed erosion of 1600-2500 m since 34 Ma (0.05 – 0.07 mm/yr) was reported in the trough below the Lambert glacier East Antarctica [16]. At a similar rate of 0.050 mm/yr in Valles Marineris, 8000 m of cumulated erosion (the elevation difference between the Ophir Chasma floor and the surrounding plateau) would be achieved in only ca. 160 my. However, on Earth, glacier bed erosion rate may be significantly faster.

Glacier bed erosion by several thousands of meters in Valles Marineris troughs would therefore not be exceptional, nor unrealistic in terms of required time. However, erosion of several thousand meters of glacier bed is more easily achieved by multiple cycles of ice flow, glacier bed deepening, ice melting (Earth) or sublimation (more likely in common Mars conditions), and isostatic rebound. Such a cyclicity has been observed in Antarctica and has been attributed to orbital changes [7]. Orbital cycles are exacerbated on Mars [8], due to the absence of orbit stabilization by a heavy natural satellite such as the Earth's Moon. Multiple glacial erosion cycles, the terms of which remain to be explored, may have vigorously contributed to erosion and deepening of the Ophir Chasma floor.

Wind. ILD fluting indicates aeolian erosion of the chasma walls around the ODS, and dark dunes are abundant on chasma floor. ILD material is weak [9] but mafic dykes are much more resistant to wind erosion. It is unclear how efficient wind-carving may have been in ODS exhumation.

5. Conclusion

Erosion, probably subglacial erosion, may have been the main mechanism by which Ophir Chasma formed. The dyke density on the Ophir Chasma floor testifies, however, to significant crustal dilation, implying significant extensional tectonics too. The first step in the formation of Ophir Chasma is thus interpreted to have been dyke dilation and tectonic stretching, then glacier bed erosion, resulting in several kilometers of additional topographic lowering. Other Valles Marineris northern chasmata might have formed in a similar way.

Acknowledgements

This work was funded by the OPUS/V-MACS project no. 2015/17/B/ST10/03426 of the National Science Centre, Poland.

References

[1] Schultz, R.A.: Planet. Space Sci., Vol. 46, pp. 827–834, 1998. [2] Rodriguez, A. and van Bergen, M.J.: Geol. Mijnbouw, Vol. 95, pp. 1–17, 2016. [3] Wilson, L. and Head, J.W.: Rev. Geophysics, Vol 32, pp. 221–263, 1994. [4] Mège, D. and Bourgeois, O. Earth Planet. Sci. Lett., Vol. 310, pp. 182–191, 2011. [5] Gourronc, M., et al.: Geomorphology, Vol. 204, pp. 235–255, 2014. [6] Smith, A.M. et al. Geology, Vol. 35, pp. 127–130, 2007. [7] Pekar, S.F. and DeConto, R.,M.: Palaeogeogr., Palaeoclim., Palaeoecol., Vol. 231, pp. 101–109, 2006. [8] Laskar., J., et al. Icarus, Vol. 170, pp. 343–364, 2004. [9] Sowe, M., et al., Lunar Planet. Sci. Conf. XXXVIII, Abstract #1568, 2007.

EPSC Abstracts
Vol. 11, EPSC2017-440-2, 2017
European Planetary Science Congress 2017

Venus Monitoring Camera (VMC/VEx) 1 micron emissivity and Magellan microwave properties of crater-related radar-dark parabolas and other terrains

A.T. Basilevsky[1,2], **O. S. Shalygina**[2], N.V. Bondarenko[3,4], E.V. Shalygin[2], and W.J. Markiewicz[2]
[1]Vernadsky Institute of Geochemistry and Analytical Chemistry, RAS, Moscow, Russia, [2]Max-Planck-Institut für Sonnensystemforschung, Göttingen, Germany (shalygina@mps.mpg.de), [3]University of California — Santa Cruz, Santa Cruz, CA, USA, [4]Institute of Radiophysics and Electronics, National Academy of Sciences of Ukraine, Kharkiv, Ukraine

1 Data description and the method of investigation

About 10 % of impact craters seen in the Magellan radar images of Venus have associated radar-dark parabolas [1, 2]. The aim of this work is a comparative study of several typical radar-dark parabolas, the neighboring plains and some other geologic units seen in the study areas, at two depths scales: the upper several meters of the study object are available through the Magellan-based microwave (at 12.6 cm wavelength) properties (microwave emissivity, Fresnel reflectivity, large-scale surface roughness, and radar cross-section), and the upper hundreds microns of the object are characterized by 1-μm emissivity resulted from the analysis of the near infra-red (NIR) irradiation of the night-side of the Venusian surface measured by the Venus Monitoring Camera (VMC) on-board of Venus Express (VEx).

Microwave parameters and 1-μm emissivity of the surface materials have been studied in five $\sim 1600 \times 1600$ km areas, which include craters Adivar, Bassi, Bathsheba, du Chatelet and Sitwell (see fig. 1), all with associated radar-dark parabolas (see an example in fig. 2). Selected for the analysis surface units include "homogeneous" and "heterogeneous" parabola parts, the non-parabolic halo of the crater Caccini (near the crater du Chatelet), plains, massifs of the tesserae terrain, and a locality of the rifted terrain in the area of crater Sitwell. The study addresses following questions about parabola formation: what is physical and geological states of various parts of parabolas; what physical and chemical changes of the material, being a source for the parabola (upper 100's meters of the plains-forming basalts), took place in the parabola formation process and their subsequent evolution [3].

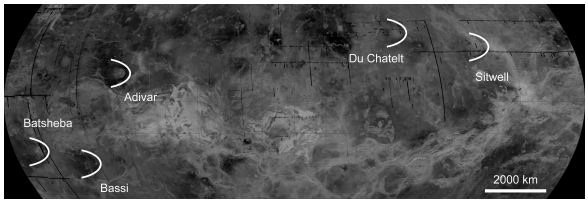

Figure 1: Locations of the dark-parabola craters under study in the Magellan synthetic aperture radar (SAR) image covering area 30°S – 40°N and 40°E – 220°E

For all mentioned above units and subunits the microwave parameters and 1-μm emissivity have been calculated and then compared. 1-μm emissivity depends on chemical and mineralogical composition of the studied materials and on the surface structure and grain size. Microwave emissivity and Fresnel reflectivity are controlled by dielectric permittivity of the surface material: the higher dielectric permittivity, the higher Fresnel reflectivity and the lower microwave emissivity.

2 Results

The comparative study of parabolas of five craters allowed coming to following conclusions:

1. 1-μm emissivity usually exhibits the dependence: the lower 1-μm emissivity, the lower Fresnel reflectivity, the higher microwave emissivity.

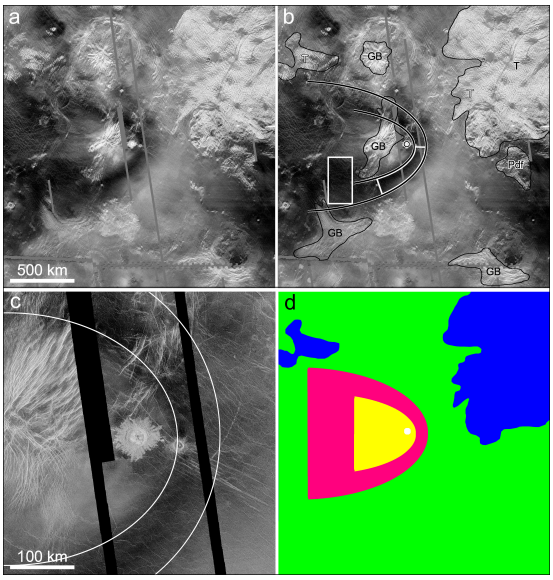

Figure 2: a) Magellan SAR image of the crater Bathsheba parabola and its vicinity; b) similar image with boundaries of the dark parabola, groove belt (GB) and tesserae terrain (T); homogeneous part of the radar-dark parabola (DHM) are outlined with white; c) Magellan SAR image of the crater Bathsheba and its close vicinity; d) simplified map of the units under study: the plains with groove belts included (green), the radar-dark part of the parabola (red), the radar-bright part of the parabola (yellow), the tesserae terrain (blue). The considered area is 1 600 km × 1 600 km.

2. Differences in bulk properties of parabola units having the same 1-μm emissivity appear to reflect differences in a packing style of mantle material consists of particles.

3. Radar bright inner parabola parts, observed within three of five studied parabolas possibly indicate more turbulent (comparing to radar-dark parts) deposition environment, thinner parabola mantles or partial coverage of the underlying surface.

4. 1-μm emissivity values of three dark parabolas remain the same over individual parabola subunits. This suggests that characteristics of the upper several hundred microns of the dark parabola mantle is very close to each other over the whole parabola area and do not depend on the bulk properties of the total parabola mantle.

5. The non-parabolic halo of the crater Caccini exhibits characteristics close to those of the dark parabolas suggesting that in a process of shrinking of the parabola into a non-parabolic halo the considered parabola parameters remain mainly unchanged. On the other hand, 1-μm emissivity of the Caccini halo based on the comparison with the Adivar parabola shows signs for the coarser Caccini halo mantle and can be treated as a degradation state.

6. The observed differences in microwave emissivity and Fresnel reflectivity between parabolas and adjacent plains may indicate that parabola materials are more weathered with oxidation of their iron into hematite since the subsurface plains material is not easily accessible for atmosphere gases.

7. Comparisons of properties for tessera terrain and plains confirmed suggestions of the earlier works on non-basaltic composition of the tessera material.

8. Distinctive (from plains) composition of the tessera material indicates also effective downslope movement of the surface material on a rough surface of the tesserae.

9. Comparisons of the rifted terrain in the area of the crater Sitwell and plains, assuming absence of the significant topographical changes between Magellan and VEx observations, showed that high tectonic deformation is the main factor that influenced the majority of rifted terrain properties including its microwave emissivity.

References

[1] D. B. Campbell, N. J. S. Stacy, W. I. Newman, et al. In: *J. Geophys. Res.* 97.E10 (1992), pp. 16249–16277. DOI: 10.1029/92JE01634.

[2] A. T. Basilevsky and J. W. Head. In: *J. Geophys. Res.* 107.E8 (2002), p. 5061. DOI: 10.1029/2001JE001584.

[3] N. V. Bondarenko and J. W. Head. In: *J. Geophys. Res.-Planets* 109.E9 (2004), E09004. DOI: 10.1029/2004JE002256.

EPSC Abstracts
Vol. 11, EPSC2017-456-1, 2017
European Planetary Science Congress 2017

Numerical simulations of multiple and single channel rivers on Earth and Titan

K. Misiura and L. Czechowski
Institute of Geophysics, University of Warsaw, Poland (kasiazlowodzka@gmail.com / Fax: +48-22-5546882)

Abstract

On Titan surface we can expect a few different geomorphological fluvial forms, e.g. fluvial valley and river channels. In present research we use numerical model of the river (Fig. 1) to determine the ranges of different fluvial parameters important for evolution of the rivers on Titan and on Earth. We have found that transport of sediments by suspended load is the main way of transport for Titan [1]. We also determined the limit of the river's parameters for which multiple-channel rivers are developed rather than single-channel rivers on the Earth [2] and on Titan.

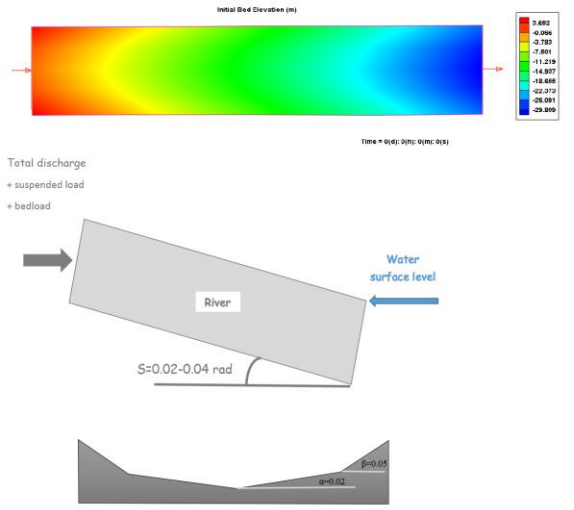

Fig. 1 The initial bed topography and other information about domain used for our simulations. The slope (*S*) of the river valley is *S*=0.01-0.04, length of the valley is 1 km, and width is 200 m. These parameters of the valley are based on the observation of rivers network at the Huygens landing site, during its descent [3]. Upper panel – topography, middle panel – cross section along the river, lower panel – cross section across the river

1. Introduction

Titan is the only moon that has dense atmosphere and flowing liquid on its surface. The Cassini-Huygens mission has found on Titan meandering river valleys, and processes of erosion, transport of solid material and its sedimentation. In this work we investigate the similarity and differences between fluvial processes on Titan and the Earth.

2. Numerical model

The dynamical analysis of the considered rivers is performed using the package CCHE modified for the specific conditions on Titan. The package is based on the Navier-Stokes equations for depth-integrated two dimensional, turbulent flow and three dimensional convection-diffusion equation of sediment transport. For more information about numerical model see discussion in [1].

3. Parameters of the model

We performed our simulations for a few different parameters of liquid and material transported by a river. For Titan we used liquid corresponding to Titan's rain (75% methane, 25% nitrogen), for Earth - the water. Our solids are– basalt and quartz for the Earth, water ice for Titan. The rest of important parameters is presented in Tab. 1.Other parameters of our model are: inflow discharge, outflow level, grain size of sediments etc. For every calculation performed for Titan's river similar calculations are performed for terrestrial ones.

Parameter	Earth	Titan
Gravity [m s^{-2}]	9.81672	1.352
Density of the liquid [kg m^{-3}]	999.84	518
Density of the solid [kg m^{-3}]	2650 and 3000	980
Viscosity of the liquid [Pa s]	8.9 x 10^{-4}	1.51 x 10^{-4}

Tab. 1 Important parameters of the model.

4. Results and Conclusions

The results of our simulation show differences in river evolution on Titan and on the Earth. Our preliminary results indicate that suspended load is the main way of transport in simulated Titan's conditions [1].

Using numerical simulations we investigate river evolution for large *S*, i.e. larger than rivers investigated by other scientists (e.g. [4]). We obtained three main types of rivers (single channel, multiple channels and transitional).We found that the trend line for transitional rivers is a decreasing function of *Q* in space (*Q*,*S*) - Fig. 2. For large *S* the number of multichannel rivers decreases. Exponent in power function for trend line for large *S* is significantly lower than for low *S*. We found that equations of trend lines for transitional rivers obtained for Titan and Earth are similar.

Acknowledgements

We are very grateful to Yaoxin Zhang and Yafei Jia from National Center for Computational Hydroscience and Engineering for providing their program – CCHE2D.

References

[1] Lane, E. W., 1957. A study of the shape of channels formed by natural streams flowing in erodible material. MRD Sediment Series No. 9, U.S. Army Corps of Engineers, Missouri River Div., Omaha, Nebraska.

[2] Leopold, L. B., Wolman, M. G., 1957. River channel patterns: braided, meandering and straight. USGS Prof. Paper 282-B, U.S. Government Printing Office, Washington, D.C.

[3] Misiura, K., Czechowski, L., 2015. Numerical modelling of sedimentary structures in rivers on Earth and Titan. Geological Quarterly, 59(3): 565-580.

[4] Misiura, K., Czechowski, L., Witek, P. P., Bendiukova, A., 2016. The formation of single-channel and multiple-channel rivers on large slopes. Geological Quarterly, 60 (4): 0–00, doi: 10.7306/gq.1330

[5] Perron, J.T., Lamb, M.P., Koven, C.D., Fung, I.Y., Yager, E., Adámkovics, M., 2006. Valley formation on Titan. Journal of Geophysical Research, 111: E11001.

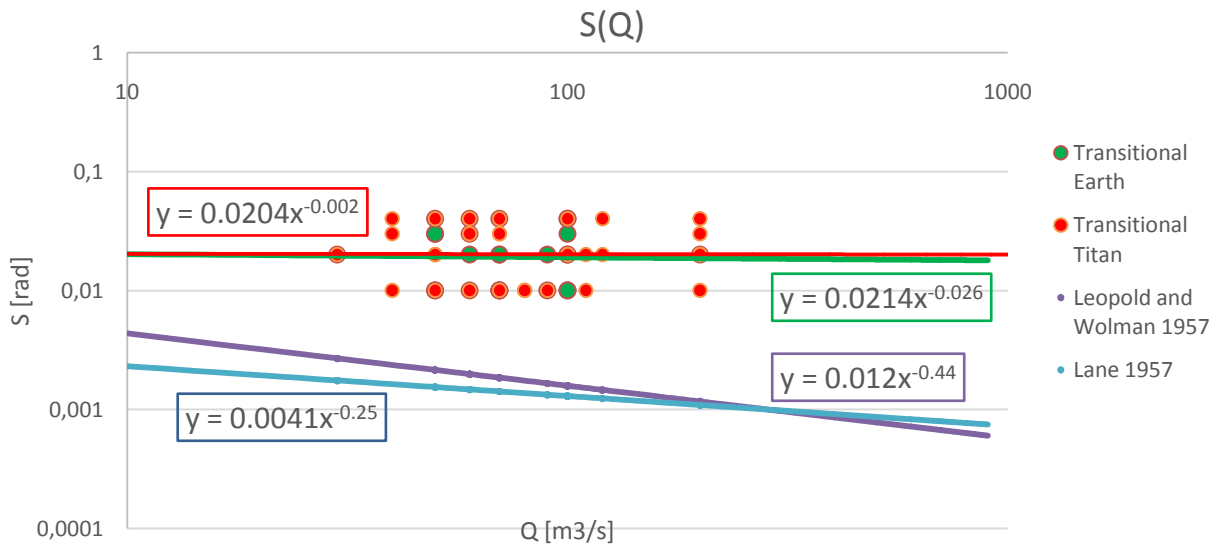

Fig. 2 Positions of simulated, transitional rivers and their trend lines (a power function) for Earth (green line) and Titan (red line) in space (*S*,*Q*), for all considered *S*. There are shown also braiding and meandering predictors of Lane (1957) and Leopold and Wolman (1957) – lines purple and blue.

EPSC Abstracts
Vol. 11, EPSC2017-473, 2017
European Planetary Science Congress 2017

High Resolution Stereo Camera (HRSC): A Geomorphological Approach

R. Jaumann (1, 2), D. Tirsch (1), S. Adeli (1), E. Hauber (1), H. Hoffmann (1), T. Roatsch (1), K. Gwinner (1), F. Preusker (1), S. Elgner (1), E. Kersten (1) and The HRSC Science Team.
(1) DLR, Inst. of Planetary Research, Berlin, Germany, Ralf.Jaumann@dlr.de. (2) Freie Universität Berlin, Inst. of Geosciences, Berlin, Germany.

The HRSC Experiment: Imagery is the major source for our current understanding of the geologic evolution of Mars in qualitative and quantitative terms. Imaging is required to enhance our knowledge of Mars with respect to geological processes occurring on local, regional and global scales and is an essential prerequisite for detailed surface exploration. The High Resolution Stereo Camera (HRSC) of ESA's Mars Express Mission is designed to simultaneously map the morphology, topography, structure and geologic context of the surface of Mars as well as atmospheric phenomena [1]. The HRSC directly addresses two of the main scientific goals of the Mars Express mission: [1] High-resolution three-dimensional photogeologic surface exploration and [2] the investigation of surface-atmosphere interactions over time; and significantly supports: [3] the study of atmospheric phenomena by multi-angle coverage and limb sounding as well as [4] multispectral mapping by providing high-resolution three-dimensional color context information. In addition, the stereoscopic imagery will especially characterize landing sites and their geologic context [1]. The HRSC surface resolution and the digital terrain models bridge the gap in scales between highest ground resolution images (e.g., HiRISE) and global coverage observations (e.g., Viking). This is also the case with respect to DTMs (e.g., MOLA and local high-resolution DTMs). HRSC is also used as cartographic basis to correlate between panchromatic and multispectral stereo data. The unique multi-angle imaging technique of the HRSC supports its stereo capability by providing 3 to 5 stereo observations from each mapping orbit, making the photogrammetric processing very robust [1,3,4]. The capabilities for three dimensional orbital by HRSC making this camera unique in the international Mars exploration effort.

Imaging Capabilities: The HRSC is a multi-sensor push broom instrument comprising 9 CCD line sensors mounted in parallel for simultaneous high resolution stereo, multicolor and multi-phase imaging by delivering 9 superimposed image swaths [1,2]. Its design permits stereo imaging with triple to quintuple panchromatic along-track stereo including a nadir-directed, forward- and aft-looking (+/-18.9°), and 2 inner (+/-12.8°) stereo line sensors. Their spectral range covers 675±90 nm. The along-track acquisition of stereo imagery reduces the influence of changes in atmospheric and illumination conditions, which so far have caused problems in the photogrammetric analysis of stereo images acquired at different observation times. The triple to quintuple stereo images permit robust stereo reconstruction, yielding Digital Terrain Models (DTMs) at a 3D accuracy better than the pixel resolution of the images.

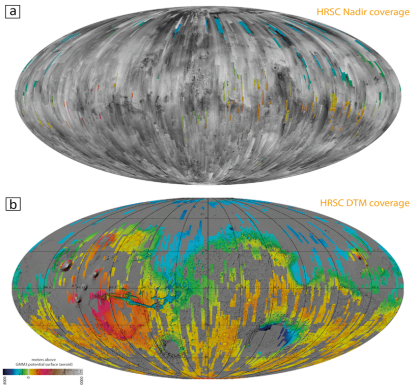

Fig. 1: HRSC coverage maps. (a) Global HRSC nadir mosaic (grey) draped onto color-coded MOLA topography. (b) Global color-coded HRSC DTM mosaic draped onto MOLA shaded relief map in grey.

The 5 panchromatic images are also used for multi-phase imaging allowing the determination of photometric surface characteristics. Multispectral imaging is realized by four line sensors in the blue, green, red and near infrared color ranges (440±45 nm, 530±45 nm, 750±20 nm, 970±45 nm). All nine lines sensors have a cross track field of view of ± 6°. They are mounted behind a single optics. High-level image processing results in radiometrically corrected and orthorectified nadir and color images as well as high

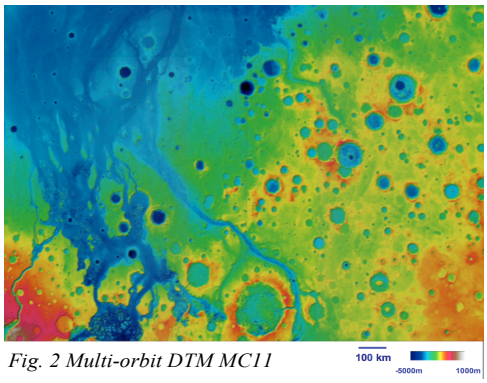

Fig. 2 Multi-orbit DTM MC11

precision DTMs (level 4), all of which are available via multiple platforms (see below). In addition, rectified images using the MOLA DTM as basis for orthorectification are produced. The individual images can be mosaicked to orthoimages of regional extent, 3D points derived from individual images are integrated into multi-orbit DTMs, and these data products can be turned into 3D-perspective views [4].

Coverage: After 13 years of orbiting the planet, HRSC has covered more than 90% of the surface with image resolutions up to 10 m/pixel. By the time of writing, the HRSC has taken more than 39.400 image sequences acquired during 4990 orbits of image acquisition flew a total of 16.882 orbits. High precision digital elevation models of up to 50 m grid spacing, generated from all suitable datasets of stereo coverage, currently cover about 50 % of the surface.

Scientific Achievements: HRSC continues yielding numerous scientific results in a variety of geological topics [e.g.5,6,7,8]. Parts of the accomplishments of the last years are collected in the Earth and Planetary Science Letters special issue "Mars Express after 6 Years in Orbit" of 2010 [e.g., 9, 10]. Recent results on the Martian Moons based on HRSC data are summarized in the 2014 PSS special issue on Phobos and Deimos [e.g.11,12,13]. The geomorphological analysis of surface features, observed by the HRSC indicate major surface modifications by endogenic and exogenic processes on all scales. Endogenic landforms (e.g., tectonic rifts, small basaltic shield volcanoes) were found to be very similar to their equivalents on Earth, suggesting that no unique processes are required to explain their formation. Volcanism may have been active up to the very recent past or even to the present, putting important constraints on thermal evolution models [13]. The analysis of diverse landforms produced by aqueous processes revealed that surface water activity was likely episodic, but ranged in age from very ancient to very recent [13]. Particularly important is prominent glaciation and periglacial features at several latitudes, including mountain glaciers [13]. The identification of aqueous alteration minerals and their geological context has enabled a better understanding of paleoenvironmental conditions and pedogenetic processes [13]. Dark dunes contain volcanic material and are evidence for the significantly dynamic surface environment, characterized by widespread erosion, transport, and redeposition [13]. Since basically all geologic interpretations of extraterrestrial features require profound knowledge of the Earth as key reference, studies of terrestrial analogues are mandatory in planetary geology. Field work in Antarctica, Svalbard and Iceland [13] provided a basis for the analysis of periglacial and volcanic processes, respectively.

Data download platforms:

http://www.rssd.esa.int/index.php?project=PSA
http://ode.rsl.wustl.edu/mars/
http://europlanet.dlr.de/mex/
http://maps.planet.fu-berlin.de
http://muted.wwu.de/
http://www.i-mars.eu/
https://jmars.mars.asu.edu/
http://www.dlr.de/dlr/en/desktopdefault.aspx/tabid-10333/

The HRSC Team: PI: R. Jaumann. Co-Is: V. Ansan, T. Basilevsky, G. Bellucci, J.-P. Bibring, M.G. Chapman, M.H. Carr, T.C. Duxbury, H. Foing, F. Fueten, S. van Gasselt, K. Gwinner, E. Hauber, J.W. Head, W.K. Hartmann, C. Heipke, H. Hiesinger, H. Hoffmann, A. Inada, W.-H. Ip, B. Ivanov, J. Jansa, H.U. Keller, R. Kirk, M. Kleinhans, P. Kronberg, R. Kuzmin, Y. Langevin, L. Le Deit, N. Mangold, W. Markiewicz, P. Masson, T.B. McCord, G.G. Michael, J.-P. Muller, J.B. Murray, J. Oberst, G. Neukum, G.G. Ori, M. Pätzold, P. Pinet, R. Pischel, T. Platz, M. Pondrelli, F. Poulet, J. Raitala, D. Reiss, A.P. Rossi, G. Schwarz, T. Spohn, S.W. Squyres, D. Tirsch, D. Williams, K. Willner.

References: [1] Jaumann R. et al. (2007) PSS, 55, 928-952. [2] Neukum G. et al. (2004), ESA Sp. Pub., SP-1240, 1-19. [3] Gwinner K. et al. (2009), PE&RS, 75(9), 1127-1142. [4] Gwinner, K. et al. (2016), PSS 126, 93-138. [5] Ansan V. & Mangold N. (2013) JGR, 118(9), 1873-1894. [6] Le Deit L. et al. (2013) JGR, 118, 1-35. [7] Hartmann W. et al. (2014) Icarus, 228, 96-120. [8] Fueten F. et al. (2014) JGR, 119, 331-354. [9] Gwinner K. et al. (2010), EPSL, 294(3-4), 506-519. [10] Jaumann R. et al. (2010), EPSL 294(3-4), 272-290. [11] Wählisch M. et al. (2014), PSS, in press, doi: 10.1016/j.pss.2013.05.012. [12] Willner K. et al. (2014), PSS, in press, doi: 10.1016/j.pss.2013.12.006. [13] Jaumann R. et al. (2015), PSS 112, 53-97.

EPSC Abstracts
Vol. 11, EPSC2017-573, 2017
European Planetary Science Congress 2017

DTM-based automatic mapping and fractal clustering of putative mud volcanoes in Arabia Terra craters

R. Pozzobon (1), F. Mazzarini (2) M. Massironi (1) G. Cremonese (3), A. P. Rossi, (4) M. Pondrelli (5) L. Marinangeli (6)
(1) Dipartimento di Geoscienze, Università degli Studi Padova, Italy (2) Istituto Nazionale di Geofisica e Vulcanologia, Pisa, Italy, (3) INAF-Osservatorio astronomico di Padova, Italy, (4) Jacobs University Bremen, Bremen, Germany, (5) IRSPS – Università D'Annunzio, Chieti-Pescara, Italy, (6) IRSPS DisputEr, Università D'Annunzio, Chieti-Pescara, Italy

Abstract

Arabia Terra is a region of Mars where occurrence of past-water manifests at surface and subsurface. To date, several landforms associated with this activity were recognized and mapped, directly influencing the models of fluid circulation. In particular, within several craters such as Firsoff and an unnamed southern crater, putative mud volcanoes were described by several authors [1, 2]. In fact, numerous mounds (from 30 m of diameter in the case of monogenic cones, up to 3-400 m in the case of coalescing mounds) present an apical vent-like depression, resembling subaerial Azerbaijan mud volcanoes and gryphons [3]. To this date, landform analysis through topographic position index and curvatures based on topography was never attempted. We hereby present a landform classification method suitable for mounds automatic mapping. Their resulting spatial distribution is then studied in terms of self-similar clustering.

1. Introduction

Although the putative mud volcanoes were described in detail [2] through high-quality observations from NASA MRO HiRISE (0.25 m/pixel), a sufficient coverage among the entirety of the craters is still not available. However, CTX images at 6 m/px resolution fully cover the studied area, also presenting several overlapping observations suitable for DTM reconstruction and further analyses.

2. Methods

2.1 Stereo DTM generation

CTX stereo-derived DTMs were generated with Ames Stereo Pipeline [4] and co-registered with HRSC DTM and MOLA areoid. Since CTX DTMs have ~18 m post spacing, we developed and tested auto-detection on areas covered also by HiRISE images and DTMs (tipically at 1 m/pixel), that were subsampled at the same resolution of CTX DTM (18 m/pixel) for comparison and validation.

2.2 Mounds automatic extraction

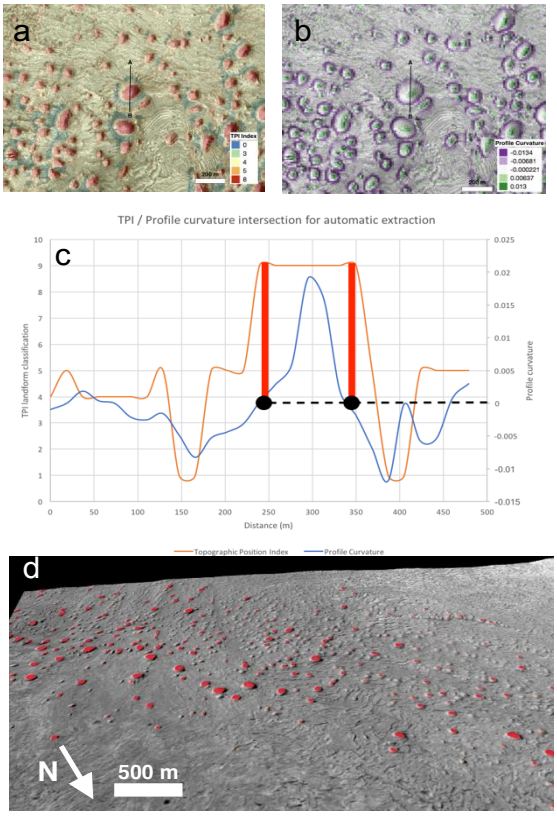

Figure 1: a) TPI index highlighting the mounds in red and their contour base in blue. In b) Profile curvature of the mounds and in c) profile curvature (blue curve) and TPI (orange curve) with the points of intersection used for automatic extraction. In d) a perspective view of mounds extracted on the southern crater

The TPI (Topographic Position Index) [5] is the basis of our morphometric classification and relies on the

difference of elevation values between a raster cell and its neighbors. The degree of relief is used to classify the DTM raster cells into slope positions [5]. Since TPI is scale dependent according to the window size, we used a multi-scale approach based on the combination of large and small window sizes to combine small positive topographic expressions with larger ones (100-1000 m)[5]. TPI values <9 were able to identify the mounds (along with ridges and yardangs) both in narrow valleys and broader plains (Figure 1). The intersection of TPI =9 with zero profile curvature was used to automatically extract the mounds' contours (Figure 1c, d). All the outliers with aspect ratio lower than 0.4 [6] (corresponding to ridges and yardangs) and smaller than 60 m (a circular feature to be detected must be at least of 4 pixels in diameter) were then discarded. All the automatically extracted features were then visually checked on HiRISE images resulting in high-precision mounds detection, and then extended on broader areas with CTX coverage.

3. Results of the Cluster analysis and future perspectives

It has been shown that on Mars percolating fractures systems be studied in terms of fractal clustering deriving the depth of fluid reservoirs [7]. In this case, the distribution of the automatically extracted mounds shows a fractal behavior up to a cutoff value that corresponds to 2 and 2.5 km deep fluid reservoir, likely feeding the putative mud volcanoes in the past (Figure 2).

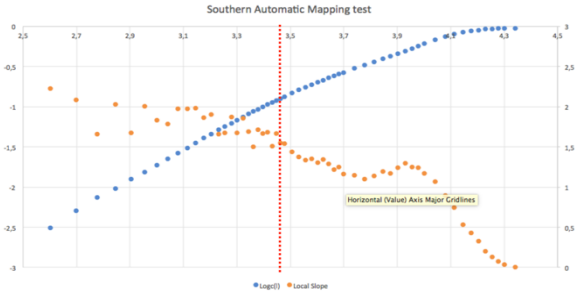

Figure 2: example mounds self-similar clustering in the southern crater based on automatic mapping. The upper cutoff of the fractal distribution is marked with the red dashed line, corresponding to 2-2.5 km of fluid source depth.

New outcomes from ExoMars TGO and CaSSIS will help to better characterize the areas in terms of morphology, composition, to provide broader DTM coverage and, possibly, clues for associated outgassing activity.

4. References

[1] Rossi, A. P., Neukum, G., Pondrelli, M., van Gasselt, S., Zegers, T., Hauber, E., Chicarro, A., and Foing, B. Large-scale spring deposits on Mars? Journal of Geophysical Research: Planets 113, no. 8 (2008).

[2] Pondrelli, M., Rossi, A.P., Ori, G.G., van Gasselt, S., Praeg, D., Ceramicola, S. Mud volcanoes in the geologic record of Mars: The case of Firsoff crater. Earth and Planetary Science Letters 304, 511–519, doi:10.1016/j.epsl.2011.02.027 (2011).

[3] Bonini, M., 2012. Mud volcanoes: Indicators of stress orientation and tectonic controls. Earth-Science Rev. 115, 121–152. doi:10.1016/j.earscirev.2012.09.002

[4] Shean, D. E., O. Alexandrov, Z. Moratto, B. E. Smith, I. R. Joughin, C. C. Porter, Morin, P. J. 2016. An automated, open-source pipeline for mass production of digital elevation models (DEMs) from very high-resolution commercial stereo satellite imagery. ISPRS Journal of Photogrammetry and Remote Sensing. 116.

[5] Weiss, A, 2001. Topographic position and landforms analysis. Poster Present. ESRI User Conf. San Diego, CA 64, 227–245.

[6] Komatsu, G., Okubo, C.H., Wray, J.J., Ojha, L., Cardinale, M., Murana, A., Orosei, R., Chan, M.A., Orm??, J., Gallagher, R., 2016. Small edifice features in Chryse Planitia, Mars: Assessment of a mud volcano hypothesis. Icarus 268, 56–75. doi:10.1016/j.icarus.2015.12.032

[7] Pozzobon, R., Mazzarini, F., Massironi, M. & Marinangeli, L., 2015. Self-similar clustering distribution of structural features on Ascraeus Mons (Mars): implications for magma chamber depth. In: Platz, T., Massironi, M., Byrne, P. K. & Hiesinger, H. (eds) 2015. Volcanism and Tectonism Across the Inner Solar System. Geological Society, London, Special Publications, 401, 203–218, doi:10.1144/SP401.12 (2014)

EPSC Abstracts
Vol. 11, EPSC2017-618-1, 2017
European Planetary Science Congress 2017

A three-dimensional geological reconstruction of Noctis Labyrinthus slope tectonics from CaSSIS data

M.Massironi (1, 2), R. Pozzobon (1), A.Lucchetti (2), E.Simioni (2, 3), C.Re (2), T. Mudrič (2), M. Pajola (4) G.Cremonese (2), A. Pommerol (5), F. Salese (6), D. Mege (7), N.Thomas (5)

(1) Dept.Geosciences and CISAS , University of Padova, Italy (matteo.massironi@unipd.it); (2) INAF, Osservatorio Astronomico di Padova, Italy; (3) CNR-Institute for Photonics and Nanotechnologies, Padova LUXOR, Padova, Italy (4) NASA Ames Research Center, Moffett Field, CA 94035, USA, (5) Physics Institute, Space Research and Planetary Sciences - University of Bern, Switzerland, (6) IRSPS, Università D'Annunzio, Chieti-Pescara, Italy, (7) Space Research Centre, Polish Academy of Sciences ul. Bartycka 18A, Warsaw, Poland

Abstract

In November 2016 the CaSSIS (Colour and Stereo Surface Imaging System [1]) imaging system onboard the European Space Agency's ExoMars Trace Gas Orbiter (TGO) acquired 18 images (each composed by 30 framelets for each of the 4 colour channels) of the Martian surface. The first stereo-pairs were taken during the closest approach, at a distance of 520 km from the surface, over the Hebes Chasma and Noctis Labyrithus regions. In the latter case a DTM was prepared over a north facing slope bounding to the north a 2000 m deep depression and to the south a plateau complicated by extensional fault networks [2] (Fig. 1). Such slope is characterised by a downthrown block that can be interpreted as a Deep Seated Gravitational Slope Deformation (DSGSD) sensu [3,4]. In this work we will present a 3D geological reconstruction of the phenomenon that allowed us to constrain the possible main sliding surface, the volumes involved in the gravitational process and the kinematics of the mass movement.

1. 3D topographical and geological reconstructions

The DTM was realized by the pipeline developed by the team at the Astronomical Observatory of Padova (OAPD-INAF), the procedure includes the definition of tie-points by SURF operator [5], the production of a starting disparity map based on a fast NCC [6], and an iterative sub-pixel refinement with a least square matching algorithm [7]. The 3D geological reconstruction of the DSGSD was obtained using the 3DMove software, which enabled us to wrap the images onto the DTM and interpolate the mean stratification outcropping along the upper part of the displaced mass as well as the sliding plain at its base. 3DMove provided us the possibility to restore the geological section before the downward displacement and infer the kinematics of the mass movement.

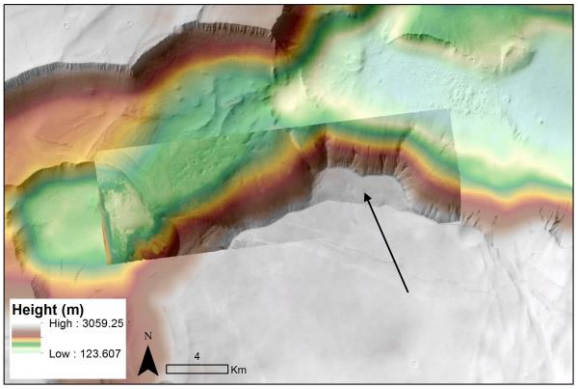

Figure 1 CaSSIS DTM in Noctis Labyrinthus over HRSC DTM. Note the downthrown block (black arrow) on the North eastern part of the CASSIS DTM .

2. Results

The CaSSIS images of the Noctis Labyrinthus acquired from the ExoMars Capture Orbit in November 2016 have revealed a DSGSD whose downward displacement exposed a 250m-high main scarp in the crown area. The displaced body does not show major internal deformations implying a still evolving en-mass sliding. The preserved stratification on the main downthrown block appear to be tilted suggesting a rotational sliding process with a gliding

surface defining a depth of the displaced mass of about 750 m (fig. 2). The upper part of the gliding surface has the same orientation of the main extensional faults transecting the plateau. This suggests a substantial structural control of the gravitational phenomena whose main gliding surface nucleated on inherited tectonic structures.

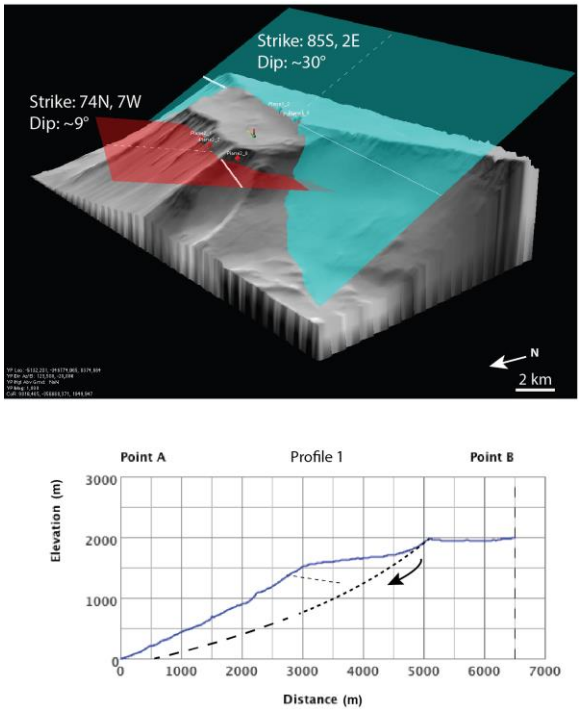

Figure 2. Top image: CASSIS DTM and interpolated planes of the stratification (red) and the upper part of the sliding surface (blue). Botton Image: geological section showing the tilted strata and the inferred gliding plain.

Acknowledgements

The authors wish to thank the spacecraft and instrument engineering teams for the successful completion of the instrument. CaSSIS is a project of the University of Bern and funded through the Swiss Space Office via ESA's PRODEX programme. The instrument hardware development was also supported by the Italian Space Agency (ASI) (ASI-INAF agreement no.I/018/12/0), INAF/Astronomical Observatory of Padova, and the Space Research Center (CBK) in Warsaw. Support from SGF (Budapest), the University of Arizona (Lunar and Planetary Lab) and NASA are also gratefully acknowledged.

References

[1] Thomas, N. et al., 2016. 47th LPSC, Abstract # 1306.

[2] Cremonese G., Simioni E., Re C., Mudric T., Lucchetti A., Massironi M., Pommerol A., Roloff V.A., Thomas N., Tornabene L.: First stereo reconstruction for the CaSSIS stereo camera on board the ExoMars Trace Gas Orbiter, LPSC, 2017

[3] Radbruch-Hall, D.: Gravitational creep of rock masses on slopes. In: Voight, B. (Ed.), Rockslides and Avalanches — Natural Phenomena. Developments in Geo- technical Engineering, vol. 14. Elsevier, Amsterdam, pp. 608–657, 1978.

[4] Crosta, G.: Landslide, spreading, deep seated gravitational deformation: analysis, examples, problems and proposals. Geografia Fisica e Dinamica Quaternaria 19, 297–313, 1996

[5] Bay et al., Comput. Vision Image Und., 110, 2008.

[6] Lewis, J.P. Vision Interface. 1995.

[7] Grün, A.. South African J. Photogramm. Re-mote Sensing and Cartography, 14, 3,1985.

EPSC Abstracts
Vol. 11, EPSC2017-674, 2017
European Planetary Science Congress 2017

ANALYSIS OF DARK SLOPE STREAKS IN NOCTIS LABYRINTHUS BASED ON MULTITEMPORAL IMAGERY AND DIGITAL ELEVATION MODEL DERIVED FROM HRSC, CTX and MOC DATA

B. P. Schreiner[1] (bjoern.schreiner@fu-berlin.de), S. H. G. Walter[1], S. van Gasselt[2], J.-P. Muller[3], P. Sidiropoulos[3]; [1]Planetary Sciences and Remote Sensing Group, Institute of Geological Sciences, Freie Universität Berlin, Germany; [2]University of Seoul, South Korea; [3]Mullard Space Science Laboratory, University College London, United Kingdom

Abstract

Recurring slope lineae (RSL) on Mars are dark and narrow downhill oriented surface features found in equatorial regions [1] associated with water or hydrated salt flows [2]. On the other hand there are Dark Slope Streaks which seem to be dry avalanches on dust covered slopes [3]. The origin of both ist still under discussion. We found linear features in eastern Noctis Labyrinthus region (6°S, 265°E) with lengths of up to several kilometres and lateral extensions of 20-30 metres. As described by [4], RSL fade and recur in the same location over multiple Mars years. Similarily, Dark Slope Streaks form on at least annual to decade-long timescales [5]. During 10 years of HRSC observation time (2005-2015) several linear features in Noctis Labyrinthus changed in visibility. Slope parameters and seasonal illumination conditions [6] are investigated based on a digital elevation model derived from HRSC data. For large datasets a feature identification is presented which involves spatial filtering in conjunction with elevation data analysis.

Data and Methods

For analysing the time sequence a number of HRSC orbits covering the Labyrinthus Noctis region have been projected to a common centre. Orbits with their corresponding ground resolution are #1955 (12.5m), #1977 (12.5m), #2402 (25m), #a497 (50m) and #e632 (12.5m). Their recording dates span approx. 10 years (July 2005 to July 2015). From these orbits a mosaicked digital terrain model has been calculated to obtain topographic information (Fig. 1). In addition to HRSC data we locally used CTX/HiRISE and MOC image data.
Dark streaks have been identified by the following steps: First the nadir image is highpass-filtered (7x7), from which a two-level image can be derived by thresholding. A sequence of morphological filters are applied (opening, closing, thinning) to produce a skeleton where features are reduced to one-pixel sized chains. These are searched for connectivity with a recursive algorithm that at the same time searches for deviation from the steepest gradient, as dark streaks are known for producing a track downslope. Only chains following the steepest gradient are kept in the record as they are candidates for dark streaks. These chains are then expanded again from their skeleton to the feature seen in the threshold image (Fig. 3).

Results

For 17 dark slope streaks with change (Fig. 2) we found life times that span from less then 1204 days to a maximum of less than 10 years, while recording dates are not equally distributed and image resolution varies from 12.5m to 50m (nominally). This results in uncertainties of detection. Also, in shadowed areas features are difficult to identify as dark streaks can be faint and rendered invisible here.
The detection of dark streaks works satisfying provided that sufficient contrast and resolution is given and a corresponding DTM is available. Still some refinement needs to be done to detect feature change between different orbits for dark slope streaks fully automatic.

Acknowledgements

The research leading to these results has received funding from the European Union's Seventh Framework Programme (FP7/2007-2013) under iMars grant agreement no. 607379.
Acknowledgements to Dominik Neu[1] for Level-4 image and DTM processing.

Figures

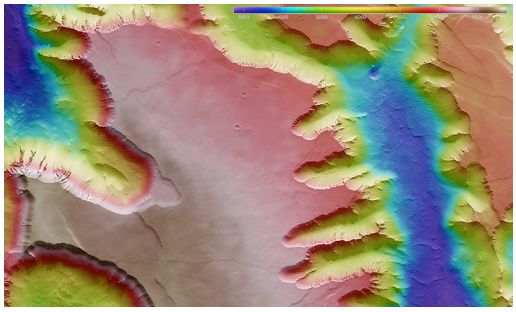

Fig. 1: Colour coded Terrain model of HRSC orbit e632 (Noctis Labyrinthus region), image area is approx. 120x80km with a height range of approx. 5000m, North to the right.

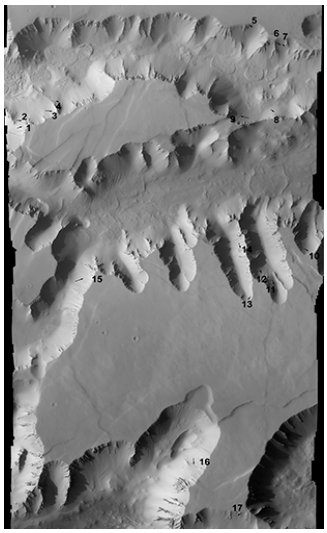

Fig. 2: Locations where dark slope streak changes appear between HRSC orbits. North is up, resolution is 12.5m/pixel.

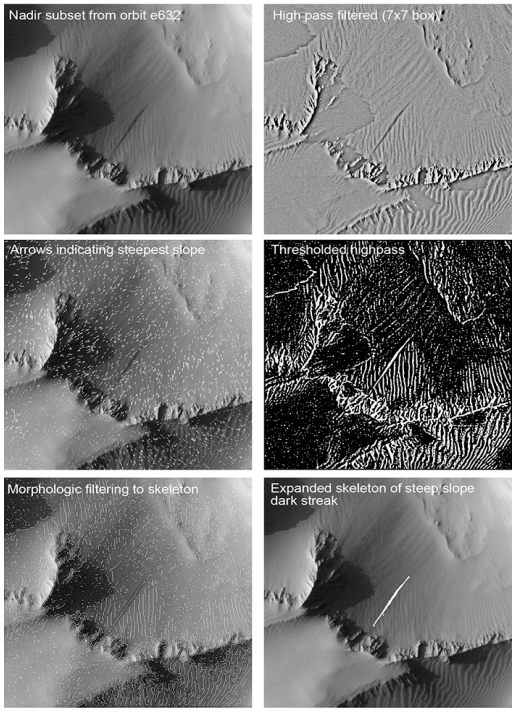

Fig. 3.: Processing steps for dark streak identification.

References

[1] McEwen, A.S., et al. (2014): Recurring slope lineae in equatorial regions of Mars. Nat. Geosci 7: 53- 58.

[2] Ojha, L. et al. (2015): Spectral evidence for hydrated salts in recurring slope linear on Mars. Nat. Geosci, DOI:10.1038/NGEO2 546.

[3] Sullivan, R. et al. (2001). Mass Movement Slope Streaks Imaged by the Mars Orbiter Camera. J. Geophys. Res., 106(E10), 23,607–23,633.

[4] McEwen, A.S., et al. (2011): Seasonal Flows on Warm Martian Slopes. Science, Vol. 333, Issue 6043, pp. 740-743.

[5] Malin, M.C.; Edgett, K.S. (2001). Mars Global Surveyor Mars Orbiter Camera: Interplanetary cruise through primary mission. J. Geophys. Res., 106(E10), 23,429–23,570.

[6] S. Walter et al. (2012): HRSC Topographic Correction by Empirical Photometric Modelling. 43rd Lun. and Plan. Sci. Conf.

EPSC Abstracts
Vol. 11, EPSC2017-739-3, 2017
European Planetary Science Congress 2017

Tracing wind tails on 67P/Churyumov-Gerasimenko

D. Tirsch (1), K. A. Otto (1), S. Mottola (1), S. Hviid (1), R. Jaumann (1,2), L. Jorda (3), E. Kührt (1), K.-D. Matz (1) and F. Preusker (1)
(1) German Aerospace Center (DLR), Institute of Planetary Research, Berlin, Germany (daniela.tirsch@dlr.de). (2) Freie Universität Berlin, Berlin, Germany. (3) Aix-Marseille Université, CNRS, Marseille, France.

Abstract

In this work we analyze wind tails on the comet 67P/Churyumov-Gerasimenko. We classify their geomorphology and examine their orientation and location. Our aim is to find out whether there exist different types of wind tails and to determine the source regions of the air-fall particles. Our results suggest erosion of particles in Ma'at and Ash regions with a particle transport from south to north.

1. Introduction

Aeolian bedforms have been detected on the surface of comet 67P/Churyumov-Gerasimenko (hereafter named 67P) by high resolution image data of the ROLIS descent imager [1] and OSIRIS orbiter camera [2] on-board the Rosetta spacecraft and its lander Philae [e.g. 3, 4, 5]. These bedforms involve dune-like landforms or ripples in the Hapi region as well as elongated deposits of granular material and semicircular depressions around several larger boulders (>5 m) resembling wind tails and moats as known from planets with atmospheres (Figure 1). Due to the similarity in morphology, we use the same terms for these bedfoms on the comet. Such features commonly form by accumulation or erosion by wind on Earth and Mars for example [e.g. 6, 7]. However, wind transport is difficult to explain on 67P and the features are probably of different origin. Nevertheless, they indicate that aeolian-like processes can transport particles across the surface of the nucleus and that this process is particularly effective where it interacts with obstacles such as boulders. Recent studies suggest that they form as a result of abrasion of a sandbed induced by air-fall particles [2, 3, 8].

1.1 Objectives

In this study, we focus on the wind tails associated with obstacles, classify their shape and appearance and track possible air-fall directions from the shape and direction of the deposits. One aim is to determine the possible source of the air-fall particles assuming that the direction of the wind tails is associated with the direction of the air-fall in the area. We base our analysis on the method described by Mottola et al. [2], which assumes that the boulders were previously covered by particles, which were subsequently eroded by impinging particles from an air-fall stream. We will compare our results with existing models of dust transport on 67P [8, 9] and will test the accordance of the models and our observations.

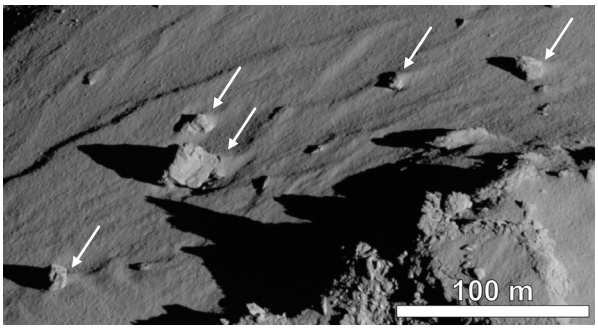

Figure 1: Examples of boulders with wind tails in the Serqet region. The wind tails point towards the upper right of the image and possess a sharp crest along the ridge. *Credit: ESA/Rosetta/MPS for OSIRIS Team MPS/UPD/LAM/IAA/SSO/INTA/UPM/DASP/IDA*

2. Methods

We investigated pre-perihelion OSIRIS images with a spatial resolution better than 50 cm/ pixel from the entire sunlit surface of the comet as well as the ROLIS descent imager data from Philae's landing site Agilkia (touch down site 1). We marked and counted all wind-tail morphologies in the image data and projected these images onto a shape model of the nucleus [10] providing a 3-dimensional view of the wind tails' orientation. For each boulder with an associated wind tail we estimated the direction of the deposit from the projected image data by determining two points on the shape model: The first point is

located where the wind tail touched the boulder and the second point is where the wind tail merges into the surrounding regolith. The connection between these two points represents the projected wind direction. In combination with the estimated boulder height (estimated to be 1/3-1/2 of the boulder width [4]), we were able to derive a preferred direction of particle in-fall associated with the abrasion of the sandbed as explained in [4].

3. Results

We found 65 wind tails on the comet's surface, which we divided into 3 morphological classes. Most of them are relatively broad and have a sharp crest along the ridge (Figure 1). Others are broad but have a rounded ridge. A small number of wind tails are elongated and slim. Most of these features are located on the small lobe in the Ma'at region, on the "head" of 67P whereas other areas are depleted (Figure 2). The average boulder size ranges around 13.5 m (±8.4 m) and the average length of the wind tails is around 13.4 m (±13.7 m). We noted a clear correlation of wind tail orientation in a given vicinity indicating a common source of the transport process. For instance, the preferred orientation of the wind tails in the Ma'at region is to the north (Figure 2). Bedforms located in other parts of the comet mostly have a different orientation indicating different source regions of the air-fall stream. The clustering of wind tails at Ma'at is consistent with the findings of [8, 9] suggesting erosion of particles in Ma'at and Ash. In addition, the orientation of the wind tails agrees with the particle transport from south to north of the comet as suggested by [10].

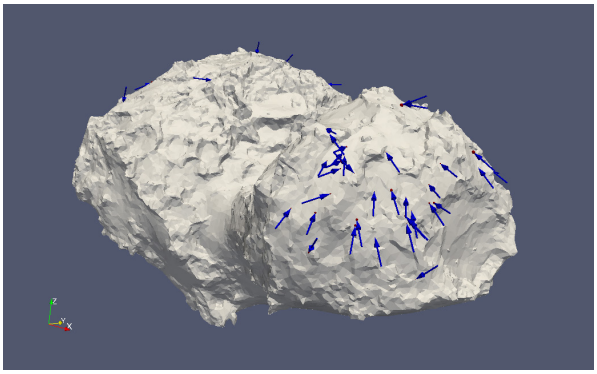

Figure 2: The location and orientation of wind tails (blue arrows) on 67P projected on a shape-model by [11]. Most of these features were found in the Ma'at region with a south to north orientation.

References

[1] Keller, H.U., Barbieri, C. Lamy, P. et al.: OSIRIS - The Scientific Camera System Onboard Rosetta, Space Science Reviews, Vol. 128, pp. 433–506, 2007.

[2] Mottola S., Arnold, G., Grotheus, H.-G., et al.: The Rolis Experiment on the Rosetta Lander, Space Science Reviews, Vol. 128, pp. 241-255, 2007.

[3] Thomas, N., Davidsson, B., El-Maarry, M.R. et al.: Redistribution of particles across the nucleus of comet 67P/Churyumov-Gerasimenko, Astronomy & Astrophysics, Vol. 583, pp. 1-18, 2015.

[4] Mottola, S., Arnold, G., Grothues, H.-G. et al.: The structure of the regolith on 67P/Churyumov-Gerasimenko from ROLIS descent imaging, Science, Vol. 349, No. 6247, pp. aab0232-1-4, 2015.

[5] Thomas, N., Sierks, H., Barbieri, C. et al.: The morphological diversity of comet 67P/Churyumov-Gerasimenko, Science, Vol. 347, No. 6220, pp. aaa0440-1-6, 2015.

[6] Greeley, R., Bridges, N.T., Kuzmin, R.O. et al.: Terrestrial analogs to wind-related features at the Viking and Pathfinder landing sites on Mars, Journal of Geophysical Research, Vol. 107, pp. 1-5, 2002.

[7] Greeley, R., Kraft, M., Sullivan, R. et al.: Aeolian features and processes at the Mars Pathfinder landing site, Journal of Geophysical Research, Vol. 104, pp. 8573-8584, 1999.

[8] Kramer, T. and Noack, M.: Prevailing dust-transport directions on comet 67P/Churyumov-Gerasimenko, Astrophysical Journal Letters, Vol. 813, 2015.

[9] Lai, I.-L., Sue, C.C. Ip, W.H. et al.: Gas outflow and dust transport of comet 67P/Churyumov-Gerasimenko. EGU General Assembly, Vienna, abstract #3655, 2016.

[10] Keller, H.U., Mottola, S., Davidsson, B. et al., Insolation, erosion, and morphology of comet 67P/Churyumov-Gerasimenko, Astronomy & Astrophysics, Vol. 583, doi: 10.1051/0004-6361/201525964.

[11] Preusker, F., Scholten, F., Matz, K.-D. et al: Shape model, reference system definition, and cartographic mapping standards for comet 67P/Churyumov-Gerasimenko - Stereo-photogrammetric analysis of Rosetta/OSIRIS image data, Astronomy & Astrophysics, Vol. 583, doi: 10.1051/0004-6361/201526349.

EPSC Abstracts
Vol. 11, EPSC2017-748-1, 2017
European Planetary Science Congress 2017

Debris Flows and Water Tracks in Continental Antarctica: Water as a geomorphic agent in a hyperarid polar desert

E. Hauber (1), C. Sassenroth (1) J.-P. de Vera (1), N. Schmitz (1), D. Reiss (2), H. Hiesinger (2), A. Johnsson (3)
(1) Institute of Planetary Research, DLR, 12489 Berlin, Germany (Ernst.Hauber@dlr.de), (2) Institut für Planetologie, Westfälische Wilhelms-Universität, 48149 Münster, Germany, (3) Göteborg University, SE-405 30 Göteborg, Sweden.

Abstract

Most studies using Antarctica as a Mars analogue have focused on the McMurdo Dry Valleys, which are among the coldest and driest places on Earth. However, other ice-free areas in continental Antarctica also display landforms that can inform the study of the possible geomorphic impact of water in a polar desert. Here we present a new analogue site in the interior of the Transantarctic Mountains in Northern Victoria Land. Gullies show unambiguous evidence for debris flows, and water tracks act as shallow subsurface pathways of water on top of the permafrost tale. Both processes are driven by meltwater from glacier ice and snow in an environment which never experiences rainfall and in which the air temperatures probably never exceed 0°C.

1. Introduction

Gullies on Mars [1] may have formed by debris flows triggered by the melting of ice or snow [2,3], by dry granular flows [4-6], or by a combination thereof. Multi-year monitoring revealed present-day mass wasting at Martian gullies, most likely related to seasonal CO_2 activity [7] in environmental conditions that prohibit the stability of liquid water. It is debated, however, whether such "dry" processes can account for the full range of morphologic characteristics and the dimensions of the observed gully systems, or whether additional "wet" processes in the recent past and in a different climate may have been required. A better physical understanding of CO_2-related (flow) processes, which have no terrestrial analogues, is required to enable predicting the geomorphic potential of such flows to generate gullies.

The study of terrestrial debris flow processes and their erosive and depositional records can help exploring the parameter space of paleo-environments that may have been responsible for gully formation on Mars. Here we introduce a new analogue site in continental Antarctica that displays evidence for debris flows in a hyperarid polar desert. The site complements our previous analogue studies in Svalbard [8], where gullies and debris flows are morphologically very similar to Martian gullies [9]. In addition, it hosts water pathways that resemble water tracks observed elsewhere in Antarctica, which were suggested to be potential analogues for the so-called RSL (recurrent slope lineae [10]).

2. Study area

The study area is located in the Transantarctic Mountains of Northern Victoria Land at the De Goes Cliff in the southernmost part of the Morozumi Range (~71°49S, 162°00E; Fig. 1). The De Goes Cliff is a ~400 m-high, east-facing scarp oriented in NNW-SSE direction, and is composed of sediments (Beacon Supergroup) and sills (Ferrar Dolerite).

The study area is very remote from any research station, and the closest weather stations are either located more towards the interior of East Antarctica or more towards the coast, respectively. Therefore, it can be reasonably assumed that the environmental conditions at the study area range between those measured at these stations. While peak summertime temperatures exceed 0°C at coastal locations on a few days in the year, the inland stations never recorded temperatures >0°C. Summertime relative humidity is ~55% at the closest weather stations (meteorological data from www.climantartide.it).

3. Observations

The geomorphology of the ice-free surfaces in the study area is characterized by glacial drift deposits and ubiquitous thermal contraction cracks. The largest ice-free area is Boggs Valley in the Helliwell

Hills, a dry valley that measures about 5 × 2.5 km in size. Trenching showed that (in January 2016) relatively clear and bubble-free ice underlies most polygonally fractured terrain at a depth of 40 cm. Katabatic winds are common and mostly blowing northward along Rennick Glacier towards the coast.

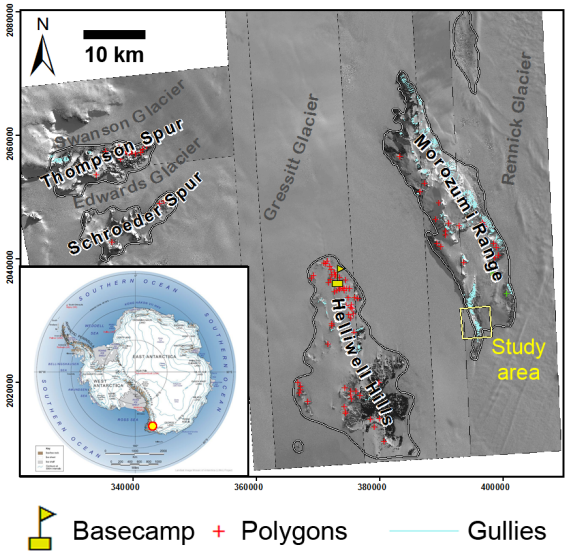

Figure 1: Location and context of study area.

3.1 Gullies.

"Gullies" (consisting from top to bottom of an erosional alcove, transport channel(s), and a depositional fan or apron, following the terminology used to describe them on Mars [1]) transect the entire height of the De Goes Cliff. Alcoves are cut into both igneous and sedimentary bedrock, followed by long and thin single-thread channels which continue across relatively small depositional fans down to the foot of the cliff. The channels are about 2 m wide and have levées that are up to 1 m wide and ~30 cm high. Debris flow tongues consist of mostly angular clasts with diameters of centimeters to decimeters. Meltwater from snow patches in the channels began to flow down the lower parts of some gullies in the early afternoon (~14:30). The length of the channel section with water flowing in it reached >13 m at 16:45, but for ~4-5 m the water only flowed in the subsurface and the surface remained completely dry. The discharge was estimated at <0.1 liter per second.

3.2 Subsurface pathways.

Immediately east of the gullies, some pathways for meltwater from snowbanks along the western margin of Rennick Glacier resemble fluvial channels in satellite images. Upon closer inspection, however, it becomes clear that these landforms do not transport flowing surface water. Instead, they represent only very shallow depressions (depth ~few cm), the surface of which is more or less wet (depending on the time since they were last active). Excavations show that the depth to ice-cemented, impermeable permafrost soil is ~40 cm. The irregular margin of the pathway (no erosion by flowing water) and the preservation of preexisting surface texture suggests that there is never any significant surface runoff in these depressions. Instead, they appear to be subsurface pathways for meltwater, just wetting the surface and darkening its albedo (analogous to *water tracks* in the McMurdo Dry Valleys [11] which, in turn, have been used as analogues to RSL [12]).

4. Discussion

We examined a new field site in Antarctica that shows landforms analogous to Martian gullies. Our observations highlight the potential of water-limited hyperarid polar deserts to generate sufficient meltwater to produce debris flows and water tracks. It appears possible that only very small amounts of water may be able to produce gullies on Mars, too. Further modeling should attempt to predict better estimates of melt rates under Martian climatic conditions that are only slightly different that those prevailing today.

Acknowledgements

We thank the Bundesanstalt für Geowissenschaften und Rohstoffe (BGR) and the expedition lead, A. Läufer, for inviting EH, JPdV and NS to the GANOVEX XI expedition in the austral summer 2015/2016.

References

[1] Malin M.C. and Edgett K.S. (2000) Science, 288, 2330–2335. [2] Costard F. et al. (2002) Science, 295, 110-113. [3] Christensen P. R. (2003) Nature, 422, 45–48. [4] Shinbrot T. et al. (2004) PNAS, 101, 8542-8546. [5] Hugenholtz C. H. (2008) Icarus, 197, 65-72. [6] Diniega S et al. (2013) Icarus, 225, 526-537. [7] Dundas C. M. et al. (2015) Icarus, 251, 244-263. [8] Hauber E. et al. (2011) GSA Spec. Pap., 483, 177-201. [9] Johnsson A. et al. (2014) Icarus, 235, 37-54. [10] McEwen A. S. et al. (2011) Science, 333, 2330-2335. [11] Levy J. S. et al. (2011) GSA Bull., 123, 2295-2311. [12] Levy J. S. (2012) Icarus, 219, 1-4.

EPSC Abstracts
Vol. 11, EPSC2017-791-1, 2017
European Planetary Science Congress 2017

Analog Experiment for Rootless Cone Eruption

R.Noguchi (1), A.Hamada (2),A.Suzuki(3) and **K. Kurita** (4)
(1) Volcanic Fluid Research Center,Tokyo Institute of Technology,Japan, (2) Central Research Inst. of Electrical Power Industry,Japan,(3) JAXA,Japan. (4) ERI,University of Tokyo, Japan (kurikuri@eri.u-tokyo.ac.jp)

Abstract

Rootless cone is one of peculiar types of pyroclastic cones, which is formed by magma-water interaction when hot lavas flow into water-logged regions. Though the occurrence on the Earth is quite limited large numbers of small cones on Mars are suspected to be rootless cones. Identification of rootless cone is crucially important in the characterization of terrane origin.To explore the formation mechanism we conducted a series of analog experiment.

1. Introduction

In planetary geology identification of rootless cone is quite crucial in the characterization of terrane origin. A lava plain composed of low viscosity lava flow is usually lack of noticeable landmarks and difficult to discriminate from other similar flows such as mud flow. Once lava plain, igneous origin is identified important implications are obtained such as the internal thermal state and activity. In this point rootless cone is a unique geomorphological signature for hot lava flow. On the martian surface there exist a plenty of rootless cones([1],[2]). They are far more abundant than the terrestrial ones. The reason is not clear. At the same time the formation of rootless cone (hereafter rootless eruption) is not fully understood. Comparing to other types of magma-water interaction such as phreatic/phreatomagmatic eruptions rootless cone eruption seems rather steady. This can be inferred from morphological comparison of the cones([3]). Phreatic/phreatomagmatic eruptions are usually violently explosive and transient while rootless cone eruption continues for a certain time steadily to form a regular cone. To understand the difference as well as the martian peculiarity we conducted analog experiments to simulate magma-water interaction by using hot syrup.

2. Experiments

The basic experimental framework to simulate the rootless eruption utilizes the reaction of thermal decomposition of sodium bicarbonate solution by touching high temperature material, which induces vesiculation of CO2 gas. The experimental procedure is as follows; we put a mixture of sodium bicarbonate powder and sugar syrup in a container at room temperature. The mass fraction of the sodium bicarbonate is changed 0 to 100 % . The viscosity of the mixture layer depends on the mass fraction. Heated condensed sugar syrup($T \sim 130^{\circ}$) is poured at the top of the mixture layer. When the heated sugar syrup gradually sinks as Rayleigh-Taylor Instability the mixture layer is gradually heated and decomposes to emit CO2 gas, which forms vesiculated structure until the temperature cools down to solidified. We measured the mass loss associated with the thermal decomposition.

3. Results

3.1. Vesiculation

Figure 1 shows variations of mass for various initial mass fractions of sodium bicarbonate. Mass decreased with time but the magnitude of mass loss shows a peculiar variation. At the mixture of 15g sodium bicarbonate-35g sugar syrup the mass loss is maximum. Figure 2 shows the amount of mass loss at 500sec. as a function of mass of sodium bicarbonate. Figure 3 displays images of vesiculated samples.The left image is for the sample of 35g sodium bicarbonate-15g sugar syrup.The right image is for the sample of 15g -35g, which corresponds to the maximum mass loss. Severe vesiculation can be seen.

3.2. Rheology

Figure 4 shows viscosity of the mixture as a function of mass of sodium bicarbonate. The viscosity values were measured at room temperature by a cone-plate type rheometer. As the amount of sodium bicarbonate

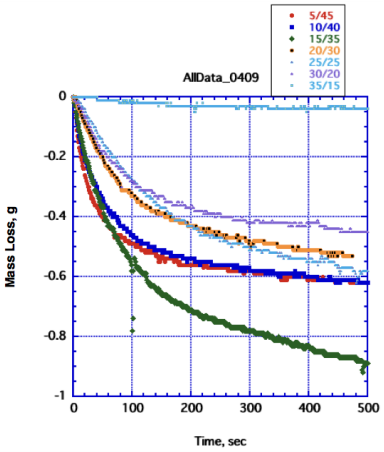

Figure 1: Variation of Mass with time.

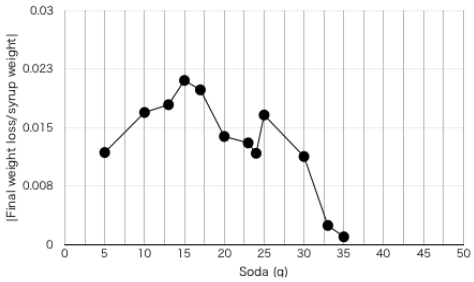

Figure 2: Amount of Mass Loss.

increases the viscosity increases and above 35 g the mixture behaves as a solid.

4. Importance of rheology

Combining the results of mass loss and rheology control of the rheology in vesiculation is remarkable. The large amount of mass loss at relatively low concentration of sodium bicarbonate(source material) shows low viscosity of the mixture can enhance the thermal decomposition. In low viscosity medium high temperature syrup can sink deeply within a limited time to cool having short scale heterogeneities at the interface. This can cause efficient mixing and heat transfer to the medium, which promotes the reaction of thermal decomposition. In rootless eruptions a similar control should be important;the rheological properties of water-logged region which is covered by hot lava flows

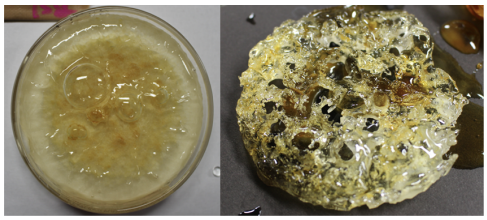

Figure 3: Photos of vesiculated sample.Left 35g sodium bicarbonate,Right 15g sodium bicarbonate

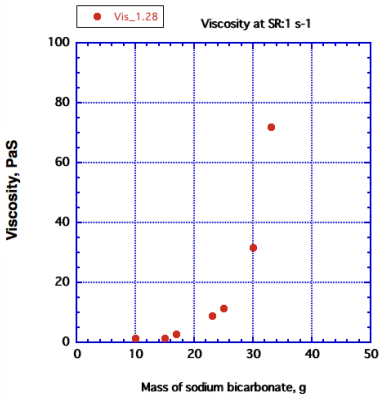

Figure 4: Viscosity

determines efficiency of mixing/contact area([1], [4]). The abundant occurrence of rootless cone on the martian surface may indicate unique properties of subsurface material rather than the terrestrial environments.

References

[1] Fagents, S. and Thodarson,: Rootless volcanic cones in Iceland and on Mars. In Geology of Mars,Cambridge Univ.Press p151-1777, 2007.

[2] Fagents,S.,Lanagan,P. and Greeley,R.: Rootless cones on Mars, Geol.Soc.London,SP202,295-317,2002.

[3] Noguchi,R.,Hoskuldsson,A. and Kurita,K.: Detailed topographical, distributional and material analyses of rootless cones in Myvatn,Iceland, J.Volcan.Geotherm.Res.,318 89-102,2016.

[4] Wohletz,K.,Zimanowski,B., and Buttner R.: Magma-water interactions, In Modeling Volcanic Processes, Cambridge Uni.Press, 230-257,2013.

EPSC Abstracts
Vol. 11, EPSC2017-839, 2017
European Planetary Science Congress 2017

Quantitative Investigations of Polygonal Patterned Ground in Continental Antarctica: A Mars analogue

C. Sassenroth, **E. Hauber**, J.P. de Vera, N. Schmitz
Institute of Planetary Research, German Aerospace Center (DLR), 12489 Berlin, Germany (Ernst.Hauber@dlr.de)

Abstract

Polygonal fractured ground is widespread at middle and high latitudes on Mars. The latitude-dependence and the morphologic similarity to terrestrial patterned ground in permafrost regions may indicate a formation as thermal contraction cracks, but the exact formation mechanisms are still unclear. This study quantitatively investigates polygonal networks in ice-free parts of continental Antarctica to help distinguishing between different hypotheses of their origin on Mars.

1. Introduction

The study site is located in the Helliwell Hills in Northern Victoria Land (~71.73°S/~161.38°E; Fig. 1) and was visited during the austral summer of 2015/2016. The surfaces are covered by glacial drift consisting of clasts with diverse lithologies. In contrast to the ancient surfaces in the McMurdo Dry Valleys, the surfaces in the study area were deglaciated since the LGM and are, therefore, relatively young. No detailed climate data are available, but data from the closest permanent weather stations suggest that the air temperatures never exceed 0°C, and that the Helliwell Hills may be considered a hyper-arid polar desert environment.

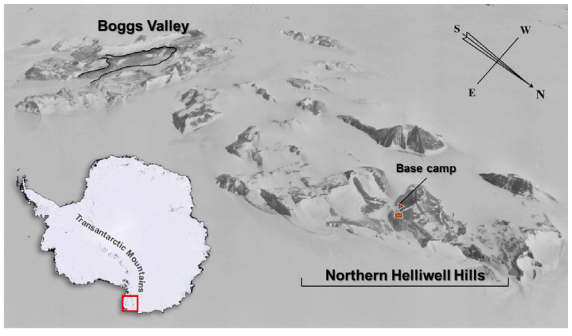

Figure 1: Location of Helliwell Hills (US Air Photo).

2. Data and Methods

Polygons were mapped in the northern part of Helliwell Hills in a GIS environment on the basis of high-resolution satellite images with a pixel size of 50 cm (Fig. 2). The measured spatial parameters include polygon area, perimeter, length, width, circularity and aspect. We also analyzed the connectivity of enclosed polygons within a polygon network and the type of polygon networks. During fieldwork, excavations were made in the center of polygons and across the bounding cracks. Soil profiles were recorded, and sediment samples were taken and analyzed for their grain size composition with laser diffractometric measurement methods.

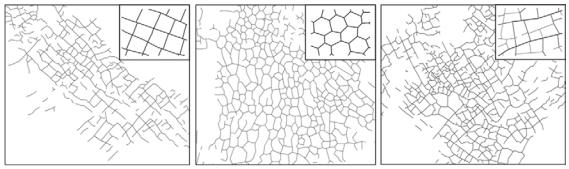

Figure 2: Examples of mapped polygon networks.

3. Observations

Thermal contraction cracks are ubiquitous in the Helliwell Hills. Polygons do not display significant local relief, but overall their centers are slightly higher than the bounding cracks (i.e. high-center polygons). Typically, the uppermost ~40 cm of regolith are dry and unconsolidated. Below that, there is commonly a sharp transition to ice-cemented material or very clear ice with few bubbles. No cracks could be identified in the ice-cemented substrate. Sizes of polygons can vary widely, dependent on the geographical location, between 10m² and >900m² (Fig. 3). In planar and level areas, thermal contraction cracks tend to be well connected as hexagonal or irregular polygonal networks (Fig. 2) without a preferred alignment. In contrast, polygonal

networks on slopes or near scarps form elongated, orthogonal primary cracks, which are either parallel or transverse to the steepest topographic gradient. Hexagonal polygon-nets tend to form smaller polygons, while polygons of orthogonal and random-orthogonal polygon-nets can form significantly larger polygons in respect to their area. Grain size analyses of the ice-free regolith (Fig. 4) show that silt dominates over clay and the coarse fraction is more abundant than the fine fraction.

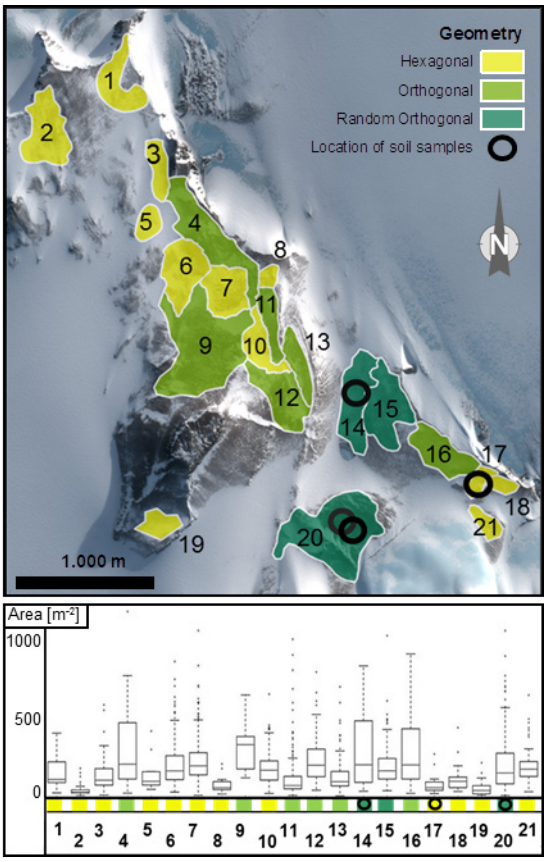

Figure 3: Different classes of polygon networks and their size sitribution (base map: WorldView-2).

4. Discussion

The geometry of the polygon-net and the geomorphometric parameters of single polygons within it correlate with the local topographic gradient. This is caused by a preferred direction of stress relief within orthogonal and random orthogonal networks, while stress release in hexagonal networks is equal in every direction. The ice cemented table does not show any visible cracks in the area below the polygon troughs. The analysis of the grain size distribution varies dependent on the locality of the excavation. There is no evidence found for some kind of sorting which would imply an ongoing process of thermal contraction within the soil.

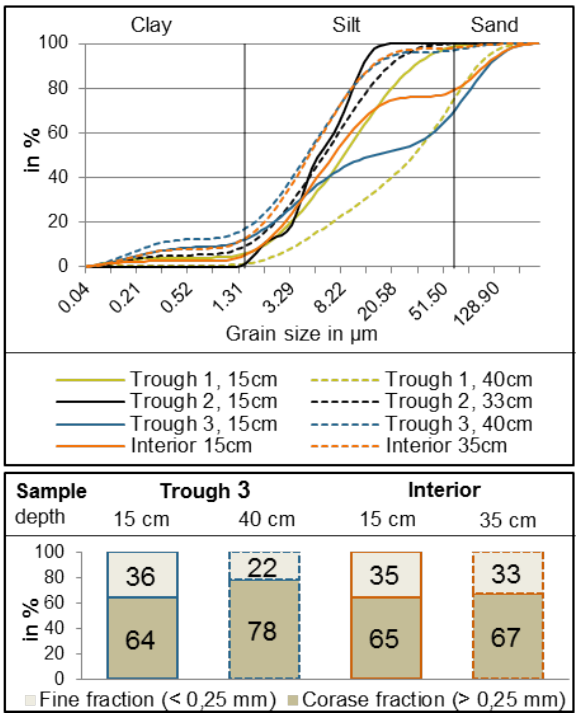

Figure 4: Grain size analysis. *(top)* Fine fraction *(bottom)* Coarse vs fine fraction within the regolith.

5. Summary and Conclusions

We conclude that the thermal contraction polygon morphometry is rather influenced by the local topography than the type of a polygon. Sublimation of ground ice, as well as minor availability of surface water, provided by melting snow, could have contributed to polygon formation in Helliwell Hills.

Acknowledgements

We thank the Bundesanstalt für Geowissenschaften und Rohstoffe (BGR) and A. Läufer as expedition leader, for inviting EH, JPdV and NS to the GANOVEX XI expedition in the austral summer 2015/2016. We appreciate the support by the DigitalGlobe Foundation which provided World View-2 images. Climate data from the Italian AWS network were kindly provided by Paolo Grigioni.

EPSC Abstracts
Vol. 11, EPSC2017-862, 2017
European Planetary Science Congress 2017

Small-scale lobes on Mars: solifluction, thaw and clues to gully formation.

A. Johnsson (1), D. Reiss (2), S.J. Conway (3), E. Hauber (4) (1) Department of Earth Sciences, University of Gothenburg, Gothenburg, Sweden (andreasj@gvc.gu.se /Fax: +46-31-786 19 86). (2) Institut für Planetologie, Westfälische Wilhelms Universität, Münster, Germany. (3) Laboratoire de Planétologie et Géodynamique, Nantes, France. (4) Institut für Planetenforschung, Deutsches Zentrum für Luft- und Raumfahrt (DLR), Berlin, Germany.

Abstract: The existence of solifluction lobe-like landforms on Mars may, potentially, have important implications for our understanding of the distribution of thaw liquids and its geomorphic effects in recent climate history. In this study we made an inventory of all HiRISE images between 40°S-80°S acquired between 2007 and 2013 and show their distribution and their close spatio-temporal relationship to other ice-related landforms such as gullies and polygons. Based on Earth-analog studies and landscape analysis we conclude that a hypothesis of freeze/thaw may better explain their origin then current ”dry” models.

1. Introduction: Small-scale lobes (SSL) on Mars are landforms that show remarkable morphologic resemblance to terrestrial solifluction lobes [1,2]. Solifluction is the net downslope movement of soil driven by phase changes of near surface water due to freeze-thaw activity [3]. SSL on Mars consists of a clast-banked arcuate front (riser) tens to hundreds of meters wide [1]. Risers are typically decimeters to a few meters (<5m) in height and the tread surface is relatively clast free [1]. SLL often display overlapping of individual lobes. Hitherto SLL's have only been studied in detail in the northern hemisphere on Mars [1,2,4-6] where they have been found to be latitude-dependent landforms [1,2]. In contrast, only a few observations have been made in the southern hemisphere [7,8]. Several authors argue for a freeze-thaw hypothesis for SSL formation on Mars [1,2,4-8]. If this interpretation is correct, the implication is significant since it would require transient H_2O liquids over large areal extents. Thus a better understanding of SLL will allow identifying environments that possibly may have experienced transient liquid water in the shallow subsurface.

This study aims to determine the distribution of SSL in the southern hemisphere and to investigate their relationship to other landforms with possible ground ice affinity such as patterned ground, polygonal terrain and gullies. Collectively, these landforms may be linked to phase changes of water at the surface or in the shallow subsurface.

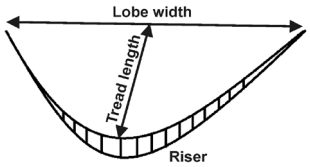

Figure 1. Sketch showing the lobe components. Lobe front points downhill.

2. Data and methods: We used images obtained by the High Resolution Imaging Science Experiment (HiRISE) that has a spatial resolution of ~25–50 cm/pixel. We catalogued and investigated all available HiRISE images that were acquired between 2007 and 2013 in the latitude band 40°S and 80°S on Mars. A total of 2200 HiRISE images have been studied in detail. For comparison to terrestrial solifluction lobes we used the airborne High Resolution Stereo Camera (HRSC-AX) [9]. The benefits of using HRSC-AX are its ability to render detailed DTM's and a similar pixel size (20 cm/pixel) as HiRISE.

3. Observations: SLL's are observed on impact crater walls. SLL's observed in HiRISE (n: 30) show a close spatial association with gullies (77%) and polygonal terrain (47% [Fig. 2]). Moreover some lobes are superposed by striped patterns (Fig. 3). Stripes were also observed separately from SLL but within the same crater environment. On Earth stone stripes and sorted stone stripes are landforms that develop in the active layer, a layer that undergoes seasonal and/or diurnal freezing and thawing. SLL's are often, but not always, associated with slopes

covered by latitude-dependent mantle (LDM) [10]. Several SLL locations show evidence of dissected mantle (26%). Moraine-like landforms were observed at ten locations (25%).

4. Discussion and conclusions: Here we show that the distribution of SLL in the southern hemisphere roughly mirrors that in the northern hemisphere distribution. Hence, SLL are hemispherically bimodal-distributed landforms, similar to polygonal terrain [e.g. 6] and gullies [e.g. 12]. However, despite more abundant sloping terrain in the southern hemisphere, fewer SLL are observed. This is in contrast to gully landforms which are more abundant in the southern hemisphere.

Martian gully landforms and their formative processes have received considerable attention in the last decade and there are currently conflicting ideas whether liquid water [e.g. 13] or CO_2–triggered mass wasting [e.g. 14] are the primary agents of erosion. As there are no CO_2 frost triggered hypotheses that can explain the occurrence of SSL, a thaw-based hypothesis could explain both landforms. In this scenario gullies and SLL may form a hydrologic continuum where available water content governs the type of landform produced. Solifluction would require ice lens formation (excess ice) to develop. Excess ice was encountered by the Phoenix Lander in 2008 [15]. Furthermore, modelling attempts may suggest that ice lenses could be widespread on Mars [16]. However more work is needed to understand the physical environment related to the CO_2 paradigm and the full suite of slope landforms predicted by it. Hence, we suggest that any model to explain gully formation must incorporate the geomorphologic context in which they occur.

Acknowledgements: This project was supported by the Swedish National Space Board.

References: [1] Johnsson et al. (2012) Icarus 21, 489–505. [2] Gallagher et al. (2011) Icarus 211, 458–471.[3] Matsuoka (2001) Earth-Sci. Rev. 55, 107–134. [3] Gallagher and Balme (2011) GSL 356, 87–111. [4] Nyström and Johnsson (2014) EPSC, #EPSC2014-480. [5] Balme et al. (2013) Prog. Phys. Geogr., 37, 289-324. [6] Mangold (2005) Icarus 174, 336-359. [7] Soare et al. (2016). Icarus 264, 184-197. [9] Jauman et al. (2007) Planet. Space Sci., 55, 928–952 [10] Mustard et al. (2001) Nature 412, 411-414. [11] Raack et al. (2012) Icarus 219, 129–141. [12] Harrison et al. (2016) Icarus 252, 236–254. [13] Conway et al. (2015) Icarus 254, 189–204. [14] Pilorget and Forget (2015) Nature Geo. 9. 65–69. [15] Mellon et al (2009). JGR-Planets 114, E003417 [16] Sizemore et al. (2015). Icarus 251, 191–210. [17] Benedict (1975) Quat. Res., 6. 55-76.

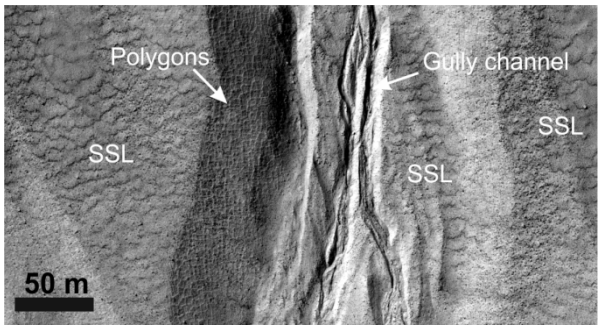

Figure 2. SLL, polygons and gullies in Ruhea crater (43.26°S/173.08°E). Fresh appearing gully channels with polygonal patterns on the gully walls. SLL dominate the scene covering the adjacent walls with overlapping lobes. The stratigraphy suggest close temporal relationship.

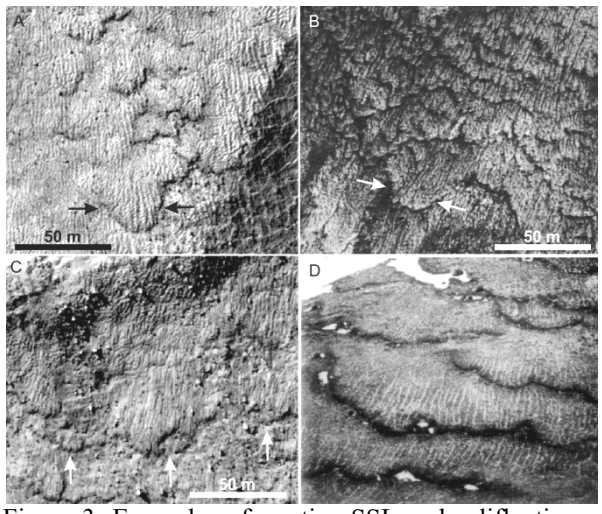

Figure 3. Examples of martian SSL and solifluction lobes on Earth. A) SSL in Ruhea crater, Mars. Overlapping lobes superposed by striped pattern. Note the polygonal terrain in lower right corner. B) Solifluction lobes superposed by stone stripes in Adventdalen, Svalbard. C) SSL in unnamed crater, Mars (45.42°S/25.74°E). Stripes are seen on the lobes. D) Solifluction lobes in New Zealand superposed by sorted stone stripes. Lobe front ~25 cm high (modified from [17])

EPSC Abstracts
Vol. 11, EPSC2017-918, 2017
European Planetary Science Congress 2017

Veiki-moraine-like landforms on Mars: Insights from analogues in northern Sweden.

A. Johnsson (1), D. Reiss (2), S.J. Conway (3), E. Hauber (4), H. Hiesinger (2), M.D. Johnson (1), M. Olvmo (1). (1) Department of Earth Sciences, University of Gothenburg, Gothenburg, Sweden (andreasj@gvc.gu.se /Fax: +46-31-786 19 86). (2) Institut für Planetologie, Westfälische Wilhelms-Universität, Münster, Germany. (3) Laboratoire de Planétologie et Géodynamique, Nantes, France. (4) Institut für Planetenforschung, Deutsches Zentrum für Luft- und Raumfahrt (DLR), Berlin, Germany.

1. Introduction: Mars is a cold hyper-arid planet where liquid water is extremely rare [1]. Most water is instead locked in a number of frozen reservoirs such as the polar caps, latitude-dependent near surface ground ice and as glacier ice. Previously, numerous studies reported on glacier landforms such as viscous flow features and lobate debris aprons where water-ice is believed to be present under insulating debris cover [2]. This notion was confirmed by SHARAD measurements [3]. However, very little is known about glacial landforms in which water is an important factor. Most studies have focused on moraine-like ridges that are associated to gully systems in crater environments [4], glacier landforms at the equatorial volcanic province [5] and drop-moraines from CO_2 glaciers [6]. Here we report on unusual irregular ring-shaped landforms within a mountain complex in Nereidum Montes, Mars. These landforms are well-preserved and may suggest recent ablation of a debris-covered, cold-based glacier. These martian ring-shaped moraine-like landforms show a striking resemblance to the Veiki moraine in northern Sweden. Veiki moraines are believed to have formed at the lobate margins of a stagnant ice-sheet during the first Weichselian glaciation [7]. The Veiki moraine is characterized by ridged plateaus that are more or less circular and surrounded by a rim ridge. The moraine complex sharply ends to the east. The newly acquired national LiDAR data over Sweden enable us studying these landforms in unprecedented detail. They also allow us exploring geomorphological similarities between Earth and Mars in large spatial contexts. This study aims to increase our understanding of glacial landforms on Mars by comparison to terrestrial analogues. Questions addressed are: (1) how morphological similar are the martian landforms to the Veiki moraine of Sweden? (2) Do the moraine-like landforms indicate the maximum extent of former ice sheets also on Mars? (3) Was any meltwater involved?

2. Data and Methods: For our study we use HiRISE (25 cm/pxl), CTX (6 m/pxl), MOLA topography and point data. CTX images have been processed using ISIS 3.0. The terrestrial analogues are covered by LiDAR. The LiDAR data have a point density between 0.5 to 1.0 points/m^2, with a footprint of 0.5 m and a scan angle of 20°. Accuracy of the z-axis is typically better than 0.1 m on flat surfaces. Field work is planned for 2017 and an forthcoming HiRISE DTM will allow for more detailed analysis of the martian landforms.

3. Observations: The martian moraine-like landforms (MLL's) are located at the end of a valley that are open in the eastward direction. In plan form the overall morphology has a distinct lobe shape (Fig. 1 A) and covers an area of approximately 80 km^2. Individual MLL's form irregular opened and enclosed ridges (Fig. 1B). By shadow measurements ridges are calculated to be 10-15 m in height. Ridges show a high concentration of boulders and clasts (Fig. 1 C). The outer lobe perimeter is mainly made up of fractured mounds. The Veiki moraines in northern Sweden show a similar irregularity of landforms forming ridged plateaus and enclosed depressions (Fig. 1D).

4. Discussion: The MLL's are located in close spatial proximity to other landforms similar in morphology to pronival rampart glaciers and cirque glaciers. The topography around the MLL's shows features that show similarities to roche moutonnées, bergschrunds (crevasses at the head of a glacier), arêtes, cols (saddle-like narrow depression formed by two head ward eroding cirques that reduce an arête) and cirques. If these interpretations are correct it shows an area with clear evidence of possibly current and former presence of glacier ice.

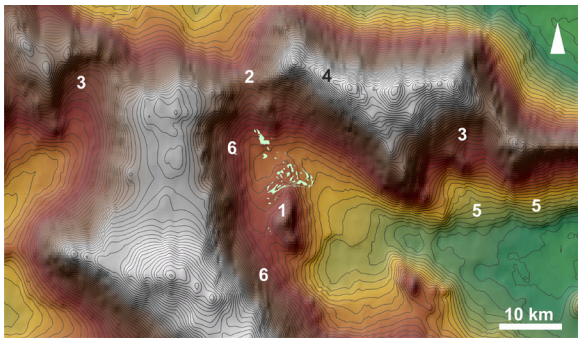

Figure 2: MOLA topographic map with 100 m contour lines and locations of possible glacial morphologies. Area located at the western part of Nereidum Montes. MLL's outlined in green dots (center). 1) Roche moutonnées. 2) Col. 3) Cirques. 4) Arête. 5) Pronival rampart. 6) Bergschrunds.

The floor of the valley, adjacent to the MLL's shows a number of exhumed impact craters which probably represent the pre-glacial surface. The very few fresh looking impact craters may point to a relatively young surface age post-glacial recession.

5. Summary: We have identified an area in the Nereidum Montes region that shows clear evidence of glaciation, including possibly preserved glacier ice and glacial landforms. This include landforms strikingly similar to the Veiki moraines of northern Sweden. A better understanding of these features may provide important insight into martian geologic and climatic history. This project is on-going and more work is needed to gain a better understanding of the sequential evolution of glacial landforms in this area.

Acknowledgements: This project has been financially supported by the Swedish National Space Board.

References: [1] McEwen et al. 2011, Seasonal Flows on Warm Martian Slopes. Science (5) 333. [2] Milliken et al., 2003. Viscous flow features on the surface of Mars: Observations from high-resolution Mars Orbiter Camera (MOC) images. JGR-Planets (E6) 108. [3] Holt et al.,2008. Radar Sounding Evidence for Buried Glaciers in the Southern Mid-Latitudes of Mars. Science (21) 322. [4] Arfstrom et al., 2005. Martian flow features, moraine-like ridges, and gullies: Terrestrial analogs and interrelationships. Icarus (2) 174. [5] Scanlon et al., 2015. PSS. [6] Head et al. 2006. Met & Plan Science (10) 41. [7] Lagerbäck, 1988. The Veiki moraines in northern Sweden-widespread evidence of an Early Weichselian deglaciation Boreas 17.

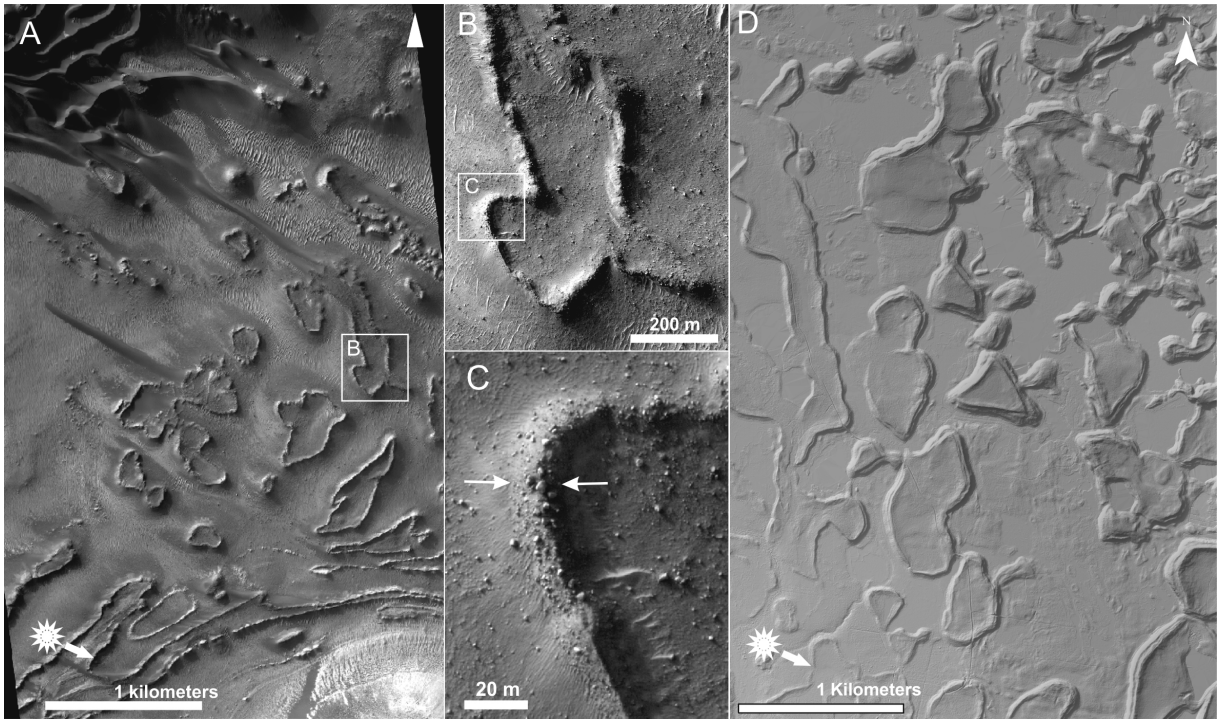

Figure 1. A) HiRISE image of multiple irregular MLL's forming a lobate pattern. B) Ridges form enclosed depressions with heights between 10-15 m. C) High clast concentrations at the ridges. D) LiDAR image of possible terrestrial analogues, called 'Veiki moraine' from northern Sweden.

EPSC Abstracts
Vol. 11, EPSC2017-932, 2017
European Planetary Science Congress 2017

Fusion of photogrammetric and photoclinometric information for high-resolution DEMs from Mars in-orbit imagery

S. Douté(1) and C. Jiang (2) (1) IPAG, Université Grenoble Alpes, Bât OSUG A CS 40700 38058 Grenoble Cedex 9 France (sylvain.doute@univ-grenoble-alpes.fr) (2) School of Geodesy and Geomatics, Wuhan University, Wuhan. China.

Abstract High-resolution Digital Elevation Models (DEMs) of the Martian surface are instrumental for studying the red planet : characterizing geological objects, generating synthetic images, normalizing illumination conditions on images, and modeling local meteorology. Our work addresses the problem of producing DEMs for regions of interest on Mars using available in-orbit imagery, typically ≈1000 km2 in area, while insuring a ≈10 meters vertical accuracy and a spatial accuracy which is comparable to that of the imagery. A method is proposed that combines photogrammetric and photoclinometric approaches in order to retain their mutual advantages. According to experiments using Mars Reconnaissance Orbiter Context Camera (CTX) images, the proposed method is indeed able to produce DEMs satisfying the previous requirements, with less artifacts, better surface continuity, and sharper details than the photogrammetric method when it is used alone.

Introduction In the literature, there are two approaches for the production of regional to local DEMs (≈10^2-10^5 km2 in area) based on images, namely photogrammetry (or stereo) and photoclinometry (or shape from shading, SFS). Photogrammetric methods need at least two images capturing the same region of interest but from a different viewpoint. It is based on the effect of parallax that can be exploited by triangulation. The core part of photogrammetry is matching, pair of pixels each belonging to one image, and solving a system of collinearity equations involving the image coordinates of the matched pixels as observations, the 3D coordinates of the corresponding point on the scene, and camera parameters. Photoclinometric methods, can derive surface gradients (i.e. slopes) from the intensity variation of an image, therefore allow to produce a DEM from a single image if the surface can be reconstructed from these gradients by integration for example. The two approaches have their own advantages and drawbacks. Photogrammetric methods are fast, able to directly produce DEMs with absolute heights and have good comparative performances for large scale objects of interest. However, the matching of pixels needs recognizable local intensity patterns on both pair images that, consequently, need to be acquired with comparable surface and illumination conditions. As for photoclinometric methods, no matching of pixels is needed, thus preserving small details in the DEM. However, the method is relatively complex and slow to converge, requires integration of gradient fields, and cannot produce absolute heights. Furthermore the modeling of intensity spatial variations in the image entails a priori information on the bidirectional reflectance properties of the surface. We propose a new fusion algorithm of photogrammetric and photoclinometric information to retain their mutual advantages.

Method Our choice is motivated by the existence of an independent, well-known and capable photogrammetric tool, which is open to public and keeps updating, i.e. NASA Ames Stereo Pipeline (ASP) (Shean et al., 2016). In the proposed algorithm (Fig. 1), the photoclinometric scheme subsequently takes this "original" DEM as an input along with the image and refines it at small scales by inverting a radiative transfer model that depicts the image intensity field for a given topography, atmospheric, illumination and viewing conditions. Another specific aspect of the algorithm is that the model is inverted with an optimization procedure containing two regularization terms. The first one insures that variables describing the height field on the one hand and the gradients on the other hand are separated for a better numerical stability. The second regularization term insures that the algorithm retains the properties of the original DEM at large scales. It also speeds up the convergence and constrains the solution space. Finally, the novelty of the proposed method is multiple. First the intensity model integrates an innovative radiative transfer scheme. Second the model also uses a realistic description of the bidirectional reflectance distribution function (BRDF) of the surface, as an anisotropic semi-empirical kernel-based model, namely the Ross-Thick Li-Sparse (RTLS) model. The

kernel weights of the RTLS model for a given scene are retrieved using the Mars-Reco algorithm (Ceamanos et al., 2013) applied to multi-angular sequences of hyperspectral images by the Compact Reconnaissance Imaging Spectrometer for Mars (CRISM) if they are available.

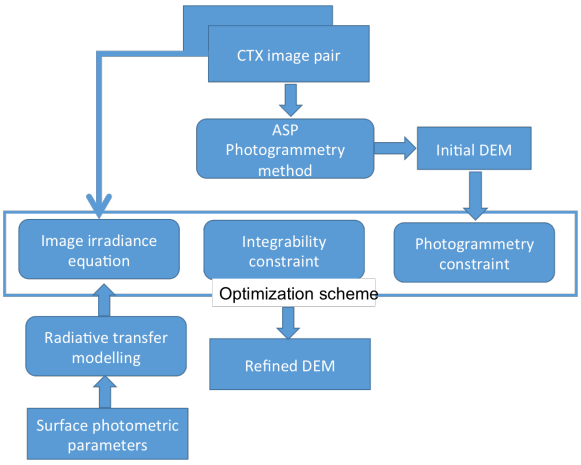

Figure 1: The flowchart of the proposed method.

Experiments and discussion

To test the proposed method, we have performed experiments with different CTX datasets of increasing complexity. By complexity we mean the fraction of missing values and the density of artifacts in the original DEM produced by ASP as well as the degree of spatial inhomogeneity and contrast affecting the intrinsic albedo of the surface. The test datasets are composed of CTX images that have been cropped according to regions of interest pixels wide so that the results are allowed to be presented in greater details. For a representative case, Fig. 2 shows results respectively obtained using only ASP and the proposed method. Individual data points collected by the Mars Orbiter Laser Altimeter (MOLA) are accessible to the public and their estimated absolute heights can be used as a reference for validating the refined DEM by calculating the Root Mean Square Error. Besides an index is calculated to evaluate the similarity of the original left CTX image and the reflectance image simulated from the refined DEM. Compared with the result using ASP, the result of the proposed method has less artifacts, its surface become more continuous, its edges become sharper and more details are revealed. The result of the proposed method also has smaller RMSE and better similarity index that stresses the consistency of its good performance.

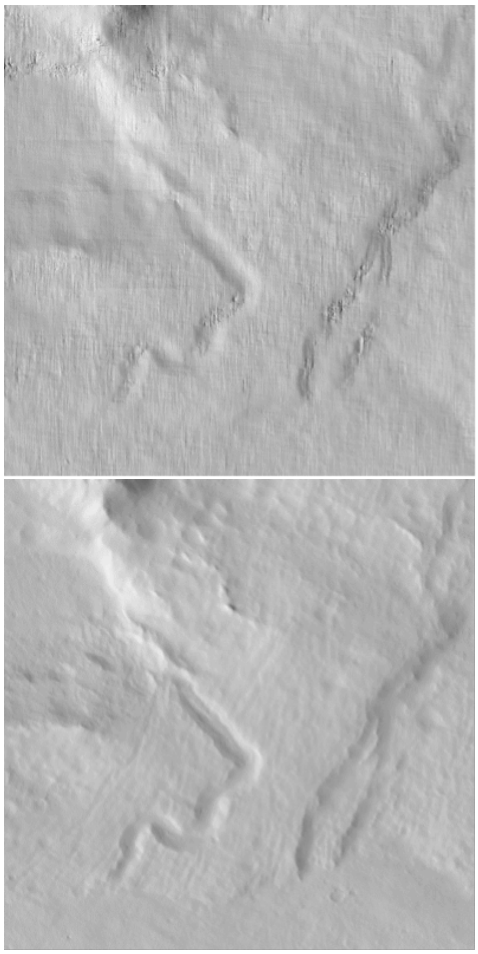

Figure 2: Results obtained using ASP only (top) and the proposed method (bottom). These shaded image sare produced when the sun azimuth is 256.63° and the sun elevation is 50.20°, same as for the left component of the CTX image pair.

Acknowledgements This research was carried out under the project " I2- Mars" conjointly funded by the Agence Nationale de la Recherche (ANR) (grant number ANR-12-IS05-0001-01) and the National Science Foundation of China (NSFC).

References

[1] X. Ceamanos et al. *JGR planets*, 118:1–20, 2013.
[2] D.E. Shean et al. In *ISPRS*, 116:101–117, 2016.